Secondary Organic Aerosol Formation from Nitrate Radical Oxidation of Styrene: Aerosol Yields, Chemical Composition, and Hydrolysis of Organic Nitrates

Yuchen Wang[1,2], Xiang Zhang[1], Yuanlong Huang[3], Yutong Liang[2,6], Nga L. Ng*[,2,4,5]

[1] College of Environmental Science and Engineering, Hunan University, Changsha, Hunan, 410082, China
[2] School of Chemical and Bimolecular Engineering, Georgia Institute of Technology, Atlanta, Georgia 30332, USA
[3] Ningbo Institute of Digital Twin, Eastern Institute of Technology, Ningbo, 315200, China
[4] School of Civil and Environmental Engineering, Georgia Institute of Technology, Atlanta, Georgia 30332, USA
[5] School of Earth and Atmospheric Sciences, Georgia Institute of Technology, Atlanta, Georgia 30332, USA
[6] Thrust of Sustainable Energy and Environment, The Hong Kong University of Science and Technology (Guangzhou), Guangdong, 511453, China
*Corresponding Author: Nga L. Ng (ng@chbe.gatech.edu)

Abstract

Styrene is emitted from anthropogenic sources and biomass burning and is highly reactive towards atmospheric oxidants. While it has the highest nitrate radical (NO_3) reactivity among aromatic hydrocarbons, the NO_3 oxidation of styrene and formation mechanisms of secondary organic aerosols (SOA) have not been investigated. In this study, we conduct chamber experiments with styrene concentrations ranging from 9.5-155.2 ppb. The resulting SOA yields range from 14.0-22.1% with the aerosol mass loadings of 5.9-147.6 $\mu g\ m^{-3}$ after wall loss corrections. The chemical composition of SOA is characterized by online measurements, revealing that dimeric organic nitrates (ONs) constitute 90.9% of the total signal of particle-phase products. $C_{16}H_{16}N_2O_8$ and $C_8H_9NO_4$ are identified as the major particle-phase products, which constitute 88.3% and 4.1% of the measured signal, respectively. We propose formation mechanisms for the ON products, including the common RO_2+RO_2/HO_2 pathway and other radical chain termination reactions such as RO+R and R+R. We also investigate the hydrolysis of particulate ONs. The hydrolysis lifetime for ONs is determined to be less than 30 minutes. This short hydrolysis lifetime can be attributed to the stabilization of the carbocation by delocalized π orbitals of the benzene-related skeleton of aromatic ONs. This work provides the first fundamental laboratory data to evaluate SOA production from styrene+NO_3 chemistry. Additionally, the formation mechanisms of aromatic ONs are reported for the first time, highlighting that compounds previously identified as nitroaromatics in ambient field campaigns could also be attributed to aromatic ONs.

1. Introduction

Aromatic hydrocarbons are a class of unsaturated chemical compounds characterized by the presence

39   of delocalized π orbitals. They play a crucial role in the atmosphere, contributing up to 60% of volatile

40   organic compounds (VOCs) in urban environments (Calvert et al., 2002; Cabrera-Perez et al., 2016).

41   Styrene is particularly unique within aromatic hydrocarbons as it possesses both an unsaturated double bond

42   and a benzene ring and has the combined properties of alkenes and aromatic compounds. Although styrene

43   is not the most abundant aromatic hydrocarbon, with concentrations ranging from 0.06 to 45 ppb in the

44   atmosphere (Cho et al., 2014; Tuazon et al., 1993), it has the highest reaction rate constants for reactions

45   with hydroxyl radicals (OH), nitrate radicals (NO_3), ozone (O_3), and chlorine radicals because of the

46   unsaturated double bond (Tuazon et al., 1993; Tajuelo et al., 2019a, b; Atkinson and Aschmann, 1988; Le

47   Person et al., 2008; Cho et al., 2014). In addition, styrene is the second most efficient aromatic hydrocarbon

48   in forming secondary organic aerosols (SOA) during daytime chemistry, surpassed only by toluene (Sun et

49   al., 2016). SOA yields from OH-initiated photooxidation of styrene can reach as high as around 35% for an

50   aerosol mass loading of 430 $\mu g/m^3$ (Schueneman et al., 2024). A theoretical study suggests that OH-initiated

51   photooxidation of styrene could be a substantial contributor to SOA formation in urban environments (Wang

52   et al., 2015).

53   To the best of our knowledge, no study has specifically investigated SOA formation from styrene+NO_3

54   oxidation. Although styrene emissions from various anthropogenic sources such as industrial activities,

55   motor vehicle operations, combustion processes, building materials, or consumer products (Zhang et al.,

56   2017; Knighton et al., 2012; Helal and Elshafy, 2012; Okada et al., 2012), are predominantly active during

57   the daytime, high levels of styrene have also been observed at night in urban environments. The nighttime

58   presence of styrene is likely influenced by the boundary layer accumulation effect (Wu et al., 2020; Lu et

59   al., 2023a), which enhances the conditions for styrene+NO_3 oxidation. Additionally, biomass burning,

60   particularly wildfires, contributes to emission of styrene in rural and forest regions (Koss et al., 2018). The

61   NO_3 oxidation of styrene can occur under conditions such as nighttime chemistry or optically dense plumes

62   during biomass burning events (Decker et al., 2021). Given that styrene exhibits the highest NO_3 reactivity

63   among aromatic hydrocarbons (Yang et al., 2020), the styrene+NO_3 oxidation can play a major role in the

64   consumption of styrene and formation of SOA.

65   The NO_3 oxidation of VOCs is also expected to generate a substantial quantity of organic nitrates

66   (ONs), primarily through the direct incorporation of the NO_3 with the double bond during reactions (Ng et

67   al., 2017; Orel et al., 1978). ONs have been shown to influence NO_x recycling, O_3 production, and the

68   formation of SOA in the atmosphere (Ng et al., 2017). Ambient field measurements consistently

69   demonstrate the widespread presence of ONs derived from aromatics in submicron organic aerosols at

70   various locations globally (Lu et al., 2023b; Lin et al., 2021; Jiang et al., 2023; Yang et al., 2019). For

71   example, in Shanghai, around 16% of the oxygenated organic molecules containing two nitrogen atoms

72   originate from aromatic compounds (Lu et al., 2023b). In Beijing, the concentration of phenethyl nitrate is

73 found to be 3.23 ng m^{-3} (Yang et al., 2019). All these suggest that the oxidation of styrene by NO$_3$ could be

74 an important pathway for generating aromatic ONs.

75   Hydrolysis of particulate ONs is an important sink of NO$_x$, especially when the ONs have short

76 hydrolysis lifetimes (Pye et al., 2015; Fisher et al., 2016; Zare et al., 2019; Vasquez et al., 2021; Takeuchi

77 and Ng, 2019). To our knowledge, there is only one study on hydrolysis of ONs formed from oxidation of

78 1,2,4-trimethylbenzene (Liu et al., 2012). More studies focus on biogenic ONs. For instance, results from

79 hydrolysis of biogenic ONs in bulk solutions indicate that the number of alkyl substitutions, the types of

80 functional groups, and the structures of carbon skeletons are three important factors controlling hydrolysis

81 rates (Darer et al., 2011; Hu et al., 2011; Jacobs et al., 2014; Rindelaub et al., 2016; Wang et al., 2021b). A

82 common feature identified in the mechanisms is the formation of stable carbocations, which facilitates the

83 rapid hydrolysis of ONs. Previous research indicates that the benzene-related skeleton, featuring three

84 delocalized π orbitals, enhances the hyper-conjugation effect and stabilizes the carbocation (Wang et al.,

85 2021b). Consequently, ONs produced from styrene+NO$_3$ oxidation, which include such benzene-related

86 skeletons, are likely to have short hydrolysis lifetimes. However, this hypothesis has not been evaluated

87 before, because of the lack of hydrolysis studies of aromatic ONs.

88   In this study, we aim to investigate SOA formation and chemical composition from styrene+NO$_3$

89 oxidation. We conduct a series of chamber experiments in the dark under both dry and humid conditions.

90 SOA yields are determined across a wide range of initial styrene concentrations under dry conditions. The

91 chemical composition of SOA is characterized by online mass spectrometry and the SOA formation

92 mechanism is proposed based on these measurements. Additionally, we investigate hydrolysis of particulate

93 ONs. These results can be used to estimate SOA formation and transformation from NO$_3$ oxidation of

94 styrene from anthropogenic emissions and biomass burning in ambient environments.

95 **2. Experimental Section**

96 **2.1. Environmental chamber experiments**

97   The experimental conditions are summarized in Table 1. All experiments are performed in the Georgia

98 Tech Environmental Chamber (GTEC) Facility, which consists of two 12 m^3 Teflon chambers (Boyd et al.,

99 2015). Experiments are conducted at 295 ± 3 K and ambient pressure. Most experiments are conducted

100 under dry conditions (RH < 3%, Exp. 1-10), with the exception of two experiments (Exp. 11 and 12), which

101 are conducted under humid conditions (approximately 50% and 70%, respectively). These humid

102 experiments allow for the investigation of the hydrolysis processes of SOA.

103   A typical experiment begins with the injection of seed particles into the chamber by atomizing a dilute

104 ammonium sulfate solution (AS; 0.015 M). Subsequently, styrene (99 %, Sigma-Aldrich) is injected into

105 the chamber using a glass bulb, where the evaporation of styrene is facilitated by the flow of zero air at a

106 rate of 5 L min^{-1} through the bulb. The initial particle number and volume concentration are 2.9×10^4

107 particles cm^{-3} and 3.2×10^{10} nm^3 cm^{-3}, respectively. The initial concentration of styrene ranges from 9.5-

108 155.2 ppb. It is noted that Exp. 9 and 10 do not involve seed particle injection and are conducted specifically

109 to determine the density of styrene+NO$_3$ SOA.

110 N$_2$O$_5$ is generated by the reaction of NO$_2$ (Matheson, 500 ppm) and O$_3$ (generated by passing purified

111 air through a UV light (Jelight 610), ~125 ppm) in a flow tube (0.8 L min^{-1} flow rate, 115 s residence time)

112 and injected into the chamber as NO$_3$ precursor, similar to our prior studies (Boyd et al., 2017; Takeuchi

113 and Ng, 2019; Takeuchi et al., 2022). The injection time ranges from 5 to 75 minutes, depending on the

114 initiation concentration of styrene. The typical styrene to N$_2$O$_5$ ratio is approximately 1:2. To ensure that

115 styrene is predominantly oxidized by NO$_3$, the concentrations of O$_3$ and the flow rates of both NO$_2$ and O$_3$

116 are adjusted (based on results from a simple kinetic box model, Table S1) to optimize N$_2$O$_5$ production

117 while minimizing O$_3$ concentration. Upon entering the chamber, N$_2$O$_5$ thermally decomposes, generating

118 NO$_2$ and NO$_3$, establishing an equilibrium that marks the onset of NO$_3$ oxidation (Boyd et al., 2015;

119 Takeuchi and Ng, 2019).

120 **2.2. Gas- and particle-phase measurements**

121 The concentrations of O$_3$ and NO$_x$ are monitored with an ultraviolet absorption O$_3$ monitor (Teledyne

122 T400) and a NO$_x$ monitor (Thermo Fisher Scientific 42C) (Teledyne 200EU), respectively. A gas

123 chromatograph with flame ionization detector (GC-FID, Agilent) is used to track the decay of styrene.

124 Aerosol volume and size distributions of particles smaller than 1 μm in electrical mobility diameter are

125 measured by a scanning mobility particle sizer (SMPS) under the low-flow mode (sheath flow of 2 L min^{-1}

126). The SMPS is consisted with a differential mobility analyzer (TSI 3080) and a condensation particle

127 counter (TSI 3775).

128 A high-resolution time-of-flight aerosol mass spectrometer (HR-ToF-AMS; Aerodyne Research Inc.)

129 is used to quantitatively measure the bulk particle-phase chemical composition including organics, nitrate,

130 sulfate, ammonium, and chloride. The working principle and operation of the HR-ToF-AMS are described

131 in detail elsewhere (DeCarlo et al., 2006). Elemental analysis of the data is conducted to determine the

132 elemental composition of the bulk aerosols (Canagaratna et al., 2015). The data are analyzed using PIKA

133 v1.16I in Igor Pro 6.38B.

134 The speciated oxidized gas- and particle-phase products are measured using a high-resolution time-of-

135 flight chemical-ionization mass spectrometer coupled with the filter inlet for gases and aerosols (FIGAERO-

136 CIMS; Aerodyne Research Inc.) with iodide (I$^-$) as the reagent ion. Details on the operation of the instrument

137 has been described in previous literature (Boyd et al., 2017; Takeuchi and Ng, 2019; Nah et al., 2016b;

138 Chen et al., 2020; Lopez-Hilfiker et al., 2014). Briefly, reagent ions are generated from a cylinder containing

139 a mixture of CH$_3$I and dry N$_2$ (Airgas) and through polonium-210 source (NRD; model P-2021). Each

140 sampling cycle lasts for 60 minutes. The instrument measures gaseous compounds by sampling air from

the chamber at 1.7 L min^{-1} for 30 minutes. At the same time, particles in the chamber are collected onto a polytetrafluoroethylene filter with the sampling rate from 1 to 5 L min^{-1} depending on the aerosol mass concentrations. A gradually heated nitrogen gas flows over the filter, evaporating oxidized organic species and transporting them into the CIMS for detection, with a temperature ramp period of 10 minutes, a soak period of 15 minutes, and a cooling phase of 5 minutes. The data are analyzed using Tofware v2.5.11. All the compounds presented in this study are I$^-$ adducts.

2.3. Volatility Calibration

In the FIGAERO-CIMS, during the thermal desorption stage, the temperature at which the maximum (T_{max}) desorption signal for a particle-phase compound is observed corresponds to effective saturation mass concentration (C*) (Lopez-Hilfiker et al., 2014; Thornton et al., 2020; Stark et al., 2017; Ylisirniö et al., 2021). The experimental procedures for volatility calibration have been described in detail in our previous study (Takeuchi et al., 2022). Briefly, the relationship between T_{max} and C* in FIGAERO-CIMS is established by depositing a mixture of standards with known C* onto the filter. These standards are then subjected to thermal desorption using the same thermal program applied in the chamber experiments. The standards used in this study include glycolic acid ($C_2H_4O_3$), oxalic acid ($C_2H_4O_2$), malonic acid ($C_3H_3O_4$), succinic acid ($C_4H_6O_4$), meso-erythritol ($C_4H_{10}O_4$), levoglucosan ($C_6H_{10}O_5$), suberic acid ($C_8H_{14}O_4$), azelaic acid ($C_9H_{16}O_4$), sebacic acid ($C_{10}H_{18}O_4$), dodecanedioic acid ($C_{12}H_{22}O_4$), palmitic acid ($C_{16}H_{32}O_2$), stearic acid ($C_{18}H_{36}O_2$), and behenic acid ($C_{22}H_{44}O_2$). The relationship between C* (in μg m^{-3}) at 25 °C and T_{max} (in °C) obtained in this study is $\log_{10} [C*_{25°C}] = -0.085T_{max} + 5.12$ (Figure S1) and is consistent with the calibrations in Takeuchi et al. (2022).

3. Results

3.1. SOA formation from NO$_3$ radical oxidation of styrene

A series of chamber experiments with different initial styrene concentrations is performed to investigate SOA formation from NO_3 oxidation of styrene (Table 1). In these experiments, the ratio of styrene to N_2O_5 is maintained at 1:2 to optimize the reaction conditions, facilitating a complete consumption of styrene and allowing for the analysis of the resulting products. Figure S2 presents the time series of the formation of SOA during a typical experiment (Exp. 7). In all experiments, styrene is fully reacted within 60 minutes, and the peak aerosol concentration is typically observed within the same time range (Figure S2).

All SOA data are corrected for particle wall loss by applying size-dependent coefficients determined from wall loss experiments (Nah et al., 2017). The nucleation experiments are conducted to determine SOA density. By comparing SMPS volume distribution and HR-ToF-AMS mass distribution (Bahreini et al., 2005; Alfarra et al., 2006; Ng et al., 2008), the SOA density is determined to be 1.35 ± 0.1 g cm^{-3}. Figure 1 shows the SOA yields (Y, 4.5%–16.1% for Exp. 1-8, over a wide range of aerosol mass loadings (ΔM_O),

175 1.9–107.4 $\mu g/m^3$). For all experiments, peak aerosol mass concentration is obtained from the SMPS aerosol

176 volume concentration (averaged over 30 minutes at peak aerosol loading) and the calculated aerosol density.

177 SOA yields are parametrized as a function of organic mass produced using the a semi-empirical model

178 (Odum et al., 1996, 1997) based on gas-to-particle partitioning of two semi-volatile products (Eq.1). The

179 fitting molar yields (α_1 and α_2) are 0.1 and 0.09, and the fitted partitioning coefficients (K_1 and K_2) are 0.4

180 and 0.02 ($R^2 = 0.997$).

$$Y = \Delta M_O \left[\frac{\alpha_1 K_1}{1 + K_1 M_O} + \frac{\alpha_2 K_2}{1 + K_2 M_O} \right]$$
                              Eq. 1

3.2. Chemical composition of SOA

183 A typical HR-ToF-AMS aerosol mass spectrum is shown in Figure 2 along with the National Institute

184 of Standards and Technology (NIST) mass spectra of possible styrene+NO_3 oxidation products. There are

185 a few notable ions in the aerosol mass spectrum. The signals at m/z 39 ($C_3H_3^+$), 50 ($C_4H_2^+$), 51 ($C_4H_3^+$), 52

186 ($C_4H_4^+$), 77 ($C_6H_5^+$), 78 ($C_6H_6^+$), 91 ($C_7H_7^+$), 105 ($C_7H_5O^+$), and 106 ($C_7H_6O^+$) are aromatic compound

187 signatures with benzene ring (McLafferty and Turecek, 1993). The signals at m/z 91 ($C_7H_7^+$), 105 ($C_7H_5O^+$),

188 and 106 ($C_7H_6O^+$), while not particularly significant in the mass spectra of other aromatic SOA systems (Yu

189 et al., 2014, 2016; Zhang et al., 2023; Liu et al., 2022; Chen et al., 2021), are relatively high for styrene+NO_3

190 oxidation system. However, m/z 91 ($C_7H_7^+$) is a signature ion for SOA formed from NO_3 oxidation of β-

191 pinene (Boyd et al., 2015) and photooxidation of β-caryophyllene (Tasoglou and Pandis, 2015). m/z 91

192 ($C_7H_7^+$) has also been detected as one of the major fragments of synthetic monoterpene ON standards

193 measured by HR-ToF-AMS (Takeuchi et al., 2024). Therefore, only m/z 105 ($C_7H_5O^+$) and 106 ($C_7H_6O^+$)

194 can potentially serve as useful indicators for SOA formed from styrene oxidation in ambient aerosol mass

195 spectra. Note that the HR-ToF-AMS spectrum of styrene+NO_3 oxidation is very similar to the NIST mass

196 spectra of benzaldehyde (C_7H_6O) and 2-hydroxy-1-phenyl ethanone ($C_8H_8O_2$). However, we do not detect

197 the prominent peaks of dimers in the HR-ToF-AMS, which can be explained by instability of dimer under

198 the high collision energy of the instrument.

199 Figure S3a presents the time series of organics and nitrate as measured by HR-ToF-AMS from a typical

200 experiment. Sulfate is used to normalize the decay of organics and nitrate because it is non-volatile and any

201 decrease in sulfate is reflective of particle wall loss and changes in aerosol collection efficiency (CE) in the

202 HR-ToF-AMS (Henry and Donahue, 2012). Organics and nitrate exhibit similar decay trends. However, the

203 situation differs when examining the time series of major organic families relative to sulfate (Figure S3b).

204 Hydrocarbon fragments (C_xH_y Family), C_xH_yO family, and $C_xH_yO_zN$ ($z>1$) family exhibit similar decay

205 rates, but decrease more rapidly relative to sulfate than C_xH_yON and $C_xH_yO_z$ families. This may indicate

206 that further aerosol aging leads to the formation of more oxidized fragments ($C_xH_yO_z$) (Boyd et al., 2015).

207 This may also suggest that the aging products are more likely to produce C_xH_yON rather than $C_xH_yO_zN$

208   fragments.

209   FIGAERO-CIMS is used to measure speciated particle-phase composition of styrene+NO_3 SOA,

210   including both dimeric and monomeric products. The characteristic SOA mass spectrum from FIGAERO-

211   CIMS (Figure 3a) is categorized according to molecule types: CHO, CHON, and $CHON_2$, each contains

212   compounds with different numbers of carbon atoms (Figure 3b). The SOA composition is dominated by

213   nitrogen-containing compounds, with $C_xH_yO_zN_2$, $C_xH_yO_zN$, and $C_xH_yO_z$ molecules constituting 91.8%,

214   7.4%, and 0.8% of the measured signal, respectively (Figure 3c). Dimers (with carbon numbers C_9 to C_{16})

215   make up 90.9% of the signal, with the majority being $C_{16}H_xO_zN_2$ dimers constituting 89.4% of the total

216   signal. Figure 4 shows the temporal evolution of major particle-phase products, the dominant product is

217    $C_{16}H_{16}N_2O_8$, contributing 88.3% of the total signal. The next most abundant particle-phase product is

218    $C_8H_9NO_4$, which constitutes 4.1% of the total signal. In addition, $C_8H_7NO_4$, $C_8H_9NO_5$, $C_8H_8N_2O_6$, and

219    $C_8H_8N_2O_7$ are major monomeric particle-phase products. $C_{16}H_{14}N_2O_8$, $C_{16}H_{17}NO_7$, $C_{15}H_{13}NO_6$, and

220    $C_{16}H_{13}NO_6$ are major dimeric particle-phase products. It is noted that it is possible that the compounds

221   detected as monomeric species are formed from the thermal decomposition process in the FIGAERO-CIMS

222   (Yang et al., 2021; Kumar et al., 2023; Stark et al., 2017).

223   **3.3. Hydrolysis of styrene-derived organic nitrates**

224   Building on results from our previous study (Wang et al., 2021b), the unique benzene-related skeleton

225   of styrene ONs can facilitate their rapid hydrolysis. Therefore, we conduct experiments with three different

226   chamber RH, including dry (RH<3%), RH~50%, and RH~70% to study the hydrolysis of styrene-derived

227   ONs. Figures S4a illustrate the time series of nitrate measured by HR-ToF-AMS for these different RH

228   systems. Distinct variations are observed in nitrate levels across different chamber RH conditions. The

229   presence of the small amounts of nitrate prior to the commencement of experiments under different RH

230   conditions could potentially result from the uptake of background nitric acid onto aqueous seed particles

231   (McMurry and Grosjean, 1985; Grosjean, 1985; Matsunaga and Ziemann, 2010; Zhang et al., 2014, 2015;

232   Yeh and Ziemann, 2015; La et al., 2016; Nah et al., 2016a; Krechmer et al., 2016; Huang et al., 2018). After

233   N_2O_5 is injected into the chamber, the large increase in nitrate in the higher RH experiments can be attributed

234   to the reactive uptake of N_2O_5 and/or the dissolution of HNO_3 into aqueous aerosols (Takeuchi and Ng,

235   2019), subsequently neutralized by ammonia to form ammonium nitrate. Therefore, to evaluate the extent

236   of particle phase ONs hydrolysis, the contributions of inorganic nitrate ($NO_{3,Inorg}$) and ONs ($NO_{3,Org}$) to the

237   measured nitrate from HR-ToF-AMS need to be separated.

238   We differentiate the contributions of $NO_{3,Inorg}$ and $NO_{3,Org}$ to the measured nitrate based on the method

239   reported in Farmer et al., (2010), as described in Eq. 2.

240                     $$x = \frac{(R_{obs} - R_{NH_4NO_3})(1 + R_{ON})}{(R_{ON} - R_{NH_4NO_3})(1 + R_{obs})}$$ Eq. 2

241   Where R_{NH4NO3} (*i.e.*, NO^+/ NO_2^+ from ammonium nitrate) is derived from the standard ionization

242   efficiency (IE) calibration of HR-ToF-AMS using 300 nm-sized ammonium nitrate particles, and the value

243   is 1.8. The R_{ON} (*i.e.*, NO^+/ NO_2^+ for ONs) value is dependent on the aerosol chemical composition and

244   instrument. The NO^+/ NO_2^+ ratio throughout all the dry experiments remains constant at approximately 4.9,

245   referred to as R_{ON} in this study. The R_{ON}/R_{NH4NO3} ratio (ratio of ratio, RoR) is 2.7, which falls within the

246   range of previous studies with the presence of ONs (Day et al., 2022). The R_{obs} value is 2.8 and 3.8 for

247   experiments with RH ~70% and 50%, corresponding to $NO_{3,Org}$ contributions of 51% and 80%, respectively.

248   Figures S4b and S5 depict the time series of $NO_{3,Org}$ for experiments under different RH. We also compare

249   the $NO_{3,Org}$ measured by HR-ToF-AMS and speciated ONs measured by FIGAERO-CIMS, which show

250   similar trends (Figure S5).

251   Here, we follow the approach reported in our previous work and used $_pON$/OA ratio to evaluate the

252   extent of ON hydrolysis via Eq. 3 (Takeuchi and Ng, 2019; Takeuchi et al., 2024). It is noted that $_pON$ refers

253   to the total mass concentration of particulate ONs, encompassing both the organic and nitrate components

254   of the ON compounds. Similarly, OA represents the total mass concentration of organic aerosols, which

255   includes both nitrated and non-nitrated organic compounds.

256 $$\frac{_pON}{OA} = \left(\frac{NO_{3,org}}{Organic+NO_{3.org}}\right) \times \left(\frac{MW_{_pON}}{MW_{NO_2,ON}}\right) = \left(\frac{\frac{NO_{3,org}}{Organic}}{1+\frac{NO_{3,Org}}{Organic}}\right) \times \left(\frac{MW_{_PON}}{MW_{NO_2,ON}}\right) \qquad \text{Eq. 3}$$

257   Where MW_{pON} refers to the average molecular weight of $_pON$ estimated from FIGAERTO-CIMS data.

258   Assuming uniform sensitivity among detected species, MW_{pON} is similar across different experiments,

259   within the range of 182.7-184.0 g mol^{-1}. $MW_{NO_2,ON}$ is the molecular weight of the nitrogen-containing

260   moiety of ONs (*i.e.*, NO_2, 46 g mol^{-1}) measured by the HR-ToF-AMS, as discussed in detail in a recent

261   study by Takeuchi et al. (2024). It is noted that given the limitation of FIGAERO-CIMS, which can lead

262   to the underestimation of simple alkyl or keto nitrates (Lee et al., 2016), as well as potential differences in

263   sensitivity among detected species, the MW_{pON} may vary.

264   As illustrated in Figure 5a, the time series of $_pON$/OA stabilizes fairly quickly, similar to what we have

265   observed previously for monoterpene systems (Takeuchi and Ng, 2019). If we utilize pseudo first-order rate

266   equations to assess the hydrolysis lifetimes at 70% RH and 50% RH, the corresponding hydrolysis lifetimes

267   are 18.8 ± 1.9 minutes and 29.5 ± 8.7 minutes for 70% RH and 50 % RH, respectively. Considering the

268   uncertainty, we report the hydrolysis lifetime to be less than 30 minutes. (Takeuchi and Ng, 2019). The

269   hydrolyzable fraction of styrene-derived ONs can be estimated from the difference in $_pON$/OA between dry

270   and RH experiments once the ratio stabilizes. The hydrolyzable fraction is about 52.7-60.6%. The observed

271   hydrolyzable ONs are $C_{16}H_{16}N_2O_8$, $C_8H_7NO_4$, and $C_8H_9NO_4$, as determined by comparing the FIGAERO-

272   CIMS mass spectra under dry and RH 70% conditions (Figure 5b). We also observe the enhancement of

273   non-nitrated organic species (*i.e.*, $C_8H_8O_5$) in the humid experiment, which could be formed from hydrolysis

274 of ONs.

4. Discussion

4.1 SOA yields over a wide range of organic mass loadings

277   There is no prior study on SOA formation from styrene+NO_3 oxidation, but previous research has
278 reported SOA formation from photolysis, OH-initiated photooxidation, and ozonolysis of styrene (Figure
279 S6). Photolysis of styrene results in the lowest SOA yields, ranging from 1.8%-3.6%, in the presence of
280 29.4 to 202.7 $\mu g/m^3$ of ΔM_O (Tajuelo et al., 2019b). Different peroxy radical (RO_2) chemistry, controlled
281 by the concentration of NO, influences the SOA formation during OH-initiated photooxidation of styrene.
282 The SOA yields are observed to be 4.0-5.0% with 174.4-348.3 $\mu g/m^3$ of ΔM_O in conditions where RO_2+NO
283 chemistry dominated (Tajuelo et al., 2019b), and around 2-35 % with 2.8-430 $\mu g/m^3$ of ΔM_O where
284 RO_2+RO_2 chemistry prevailed (Yu et al., 2022b; Schueneman et al., 2024). Several previous studies have
285 reported that the SOA yields from the ozonolysis of styrene (Ma et al., 2018; Na et al., 2006) are higher
286 than those from OH-initiated photooxidation of styrene under RO_2+NO chemistry, but lower than those
287 under RO_2+RO_2 chemistry. As shown in Figure S6, the SOA yield from the styrene+NO_3 oxidation is higher
288 than in other styrene oxidation systems when ΔM_O is lower than 80 $\mu g/m^3$.

289   Organic vapor wall loss has been reported to impact SOA yield calculation and can lead to an
290 underestimation of SOA yields by as much as a factor of 4 (McMurry and Grosjean, 1985; Grosjean, 1985;
291 Matsunaga and Ziemann, 2010; Zhang et al., 2014, 2015; Yeh and Ziemann, 2015; La et al., 2016; Nah et
292 al., 2016a; Krechmer et al., 2016; Huang et al., 2018). Therefore, to evaluate the potential effect of organic
293 vapor wall loss on SOA yields in our study, experiments without seed particles are carried out (Exp. 9 and
294 10). As show in Figure S7, the SOA formation from nucleation experiments (without seed particles) is lower
295 than condensation experiments (with seed particles). Zhang et al. (2014) determine that if organic vapor
296 wall loss is significant in chamber experiments, the addition of more seed particles will lead to an increase
297 in SOA yields. The differences in SOA formation between styrene+NO_3 nucleation experiments and
298 condensation experiments suggest the possible impact of organic vapor wall loss. Although particle wall
299 loss is accounted for, the SOA yields reported in Figure 1 and Table 1 could represent the lower limit owing
300 to vapor wall loss, where organic vapors could have partitioned to the chamber wall rather than to the
301 aerosols.

302   To account for the impact of vapor wall loss, we employ the semi-empirical equation (Eq. 1) for SOA
303 yield to correct for vapor wall loss. The correction relies on two assumptions: (1) styrene+NO_3 oxidation
304 yields two major products, and (2) the partition of these major products between gas and particle phases, as
305 well as vapor wall loss is controlled by C* of these products. The detailed procedures and the relevant
306 equations are shown in Supplementary Information (SI). The SOA yields and the SOA yield curve after this
307 correction is shown in Figure 1 and Table S2. The fitted molar yields (α_1 and α_2) are 0.8 and 0.1, and the

308 fitted partitioning coefficients (K_1 and K_2) are 8.1×10^{-4} and 7.5 (corresponding to C^* values of 1.2×10^3

309 μg/m^3 and 1×10^{-1} μg/m^3, respectively) after vapor wall loss correction (R^2=0.991). The vapor wall loss bias

310 factor, defined as the ratio of aerosol mass loadings after correction to those before correction, ranges from

311 1.3 to 3.2. The vapor wall loss bias factor is smaller for the experiments with the higher organic mass

312 loadings, consistent with results reported by Zhang et al. (2014).

313   In styrene+NO$_3$ oxidation, two products stand out in abundance, $C_8H_9NO_4$ and $C_{16}H_{16}N_2O_8$, which

314 constitute 92.4% of the total particle signal (Figure 3). We utilize two methods to estimate the C^* of

315 $C_8H_9NO_4$ and $C_{16}H_{16}N_2O_8$: the Estimation Program Interface Suite (EPI Suite) method and FIGAERO

316 thermal desorption method (Takeuchi et al., 2022). The C^* of $C_8H_9NO_4$ and $C_{16}H_{16}N_2O_8$, as simulated by

317 EPI Suite, are 1.6×10^3 μg/m^3 and 9.0×10^{-1} μg/m^3, respectively. The FIGAERO thermal desorption profiles

318 for $C_8H_9NO_4$ and $C_{16}H_{16}N_2O_8$ are shown in Figure S8. The T_{max} of $C_8H_9NO_4$ and $C_{16}H_{16}N_2O_8$ are 24.6 and

319 67.8 °C, respectively, corresponding to C^* values of 1.1×10^3 and 2×10^{-1} μg/m^3. It is noted that although the

320 FIGAERO thermal desorption profile of $C_8H_9NO_4$ shows two peaks, we use the first peak (24.6 °C) to

321 calculate the volatility, as the second peak (around 70 °C) may result from thermal decomposition of dimers

322 (Lopez-Hilfiker et al., 2016; Yang et al., 2021). The C^* of $C_8H_9NO_4$ and $C_{16}H_{16}N_2O_8$, estimated by these

323 two methods are similar to those obtained from the semi-empirical equation (Eq. 1). The consistency of the

324 C^* values across different methods supports the applicability of the semi-empirical equation (Eq. 1)

325 proposed in this study for correcting vapor wall loss in SOA yield calculation.

326 **4.2 Proposed formation mechanisms for styrene-derived organic nitrate monomers and dimers**

327   We present the proposed formation mechanisms of major particle-phase products detected by

328 FIGAERTO-CIMS (Figure 6). The formation mechanisms involve two distinct routes to generate the

329 monomeric and dimeric ONs respectively. In monomeric ONs formation pathway (Pathway A): The

330 reaction begins with the addition of a nitrooxy group (-ONO$_2$) onto the double bond of styrene follow by

331 O$_2$ addition to form a nitrooxy peroxy radical (via R1). This addition is expected to be favored because the

332 NO$_3$ radical adds to the less substituted carbon atom in the double bond. We also propose the formation

333 mechanism with NO$_3$ radical adduct to the more substituted carbon atom in the double bond in Figure S9.

334 The nitrooxy peroxy radical can further react with RO$_2$ or hydroperoxyl radical (HO$_2$) to produce the styrene

335 hydroxy nitrate ($C_8H_9NO_4$), ketone nitrate ($C_8H_7NO_4$), and peroxy nitrate ($C_8H_9NO_5$) via reactions R2, R3,

336 and R4, respectively. $C_8H_9NO_4$, which is the second most abundant product, has been observed in ambient

337 environments as well. However, it has been assumed to be nitroaromatic compounds (R-NO$_2$, *i.e.*,

338 dimethoxynitrobenzene) instead of aromatic ONs (R-ONO$_2$) (Kong et al., 2021; Wang et al., 2021a;

339 Salvador et al., 2021). $C_8H_9NO_5$ and $C_8H_7NO_4$ are also identified from residential wood-burning boilers

340 and have been suggested to be nitroaromatic compounds (Salvador et al., 2021) formed from the OH-

341 initiated photooxidation of phenolic VOCs in the presence of NO (Vione et al., 2001, 2004; Jenkin et al.,

342 2003; Frka et al., 2016; Vidović et al., 2018). Considering the ambient concentrations of nitroaromatic

343 compounds remain high even at night (Wang et al., 2019), our work suggests that styrene-derived ONs

344 could account for these molecular species in ambient environments, often only attributed to nitroaromatic

345 compounds. Furthermore, the nitrooxy peroxy radical can react with NO_3 radical to produce alkoxyl (RO)

346 radical (via R6). The RO radical can further undergo decomposition to produce benzaldehyde, benzene

347 hydroxy aldehyde, and NO_2 as the byproduct. NO_2 can react with nitrooxy peroxy radical as well through

348 reaction R5 to produce styrene peroxy nitrate ($C_8H_8N_2O_7$). Peroxy nitrate remains unstable at room

349 temperature unless there is a carbonyl group present to induce an electron-withdrawing effect, thereby

350 stabilizing the peroxy nitrooxy group (Yu et al., 2022b). Here, the benzene ring can also stabilize the peroxy

351 nitrooxy group through electron coupling (McMurry, 2012), thus promoting the formation of styrene peroxy

352 nitrate. According to Lewis and Moodie (1996), NO_3 radical can react with the double bond in olefins to

353 produce the ONs containing two nitrooxy groups. We utilize the same mechanism to elucidate the formation

354 of $C_8H_8N_2O_6$ in our work (via R7).

355   The formation of nitrogen-containing dimeric products from aromatic oxidation systems has been

356 observed in laboratory chamber studies (Molteni et al., 2018; Kumar et al., 2023; Mayorga et al., 2021).

357 For example, Kumar et al. (2023) report that dimeric products make up 54.2% of the total particle signal in

358 NO_3 oxidation of an aromatic hydrocarbon mixture, with the majority (42.3%) being $C_xH_yO_zN$ dimers.

359 Nitrated diphenyl ether dimers have been observed from the NO_3 oxidation of phenolic VOCs, as reported

360 by Mayorga et al. (2021). In our work, the predominant dimeric product is $C_{16}H_{16}N_2O_8$, which is generated

361 from RO_2+RO_2 reaction (via R8). Additionally, $C_{16}H_{14}N_2O_8$, $C_{16}H_{17}NO_7$, $C_{15}H_{13}NO_6$, and $C_{16}H_{13}NO_6$ are

362 also major dimeric ONs products observed in the particle phase. Benzaldehyde, ketone nitrate ($C_8H_7NO_4$),

363 and benzene hydroxy aldehyde, can further react with NO_3 radical via reactions R9, R10, and R11 to

364 generate radicals A1, A2, and A3, respectively. A2 and A3 can further react with each other (via R12) to

365 terminate the radical reaction by producing $C_{16}H_{13}NO_6$. Additionally, A3 can react with RO radical from

366 reaction R5 to form $C_{16}H_{14}N_2O_8$ (via R13), while A1 can react with nitrooxy peroxy radical to produce

367 $C_{15}H_{13}NO_6$ (via R14). We propose the formation of $C_{16}H_{17}NO_6$ through the reaction between nitrooxy

368 peroxy radical and styrene (via R15), followed by the RO_2 + RO_2 reaction (via R16). It is noted that in this

369 work, we propose formation mechanisms of dimeric compounds based on molecular formulas of the

370 detected species. Further experimental studies and density functional theory work are necessary to confirm

371 the structures and formation of these dimeric compounds as well as detect the critical intermediates to

372 validate the proposed mechanism.

373 **4.3 Hydrolysis of organic nitrates formed from styrene+NO_3 oxidation**

374   Condensed-phase hydrolysis has been identified as a significant sink for ONs, evidenced by substantial

375 ON uptake to aerosols and the reported short hydrolysis lifetimes (Pye et al., 2015; Fisher et al., 2016; Zare

et al., 2019; Vasquez et al., 2021). Recent studies have reported experimentally constrained parameters for the hydrolysis of biogenic ONs derived from monoterpene or isoprene, through chamber or bulk solution experiments (Takeuchi and Ng, 2019; Morales et al., 2021; Hu et al., 2011; Darer et al., 2011; Jacobs et al., 2014; Rindelaub et al., 2016; Vasquez et al., 2021; Wang et al., 2021b). Studies using bulk solutions to exam hydrolysis of ONs with specific structures have demonstrated that the number of alkyl substitutions, functional groups, and carbon skeletons are three important factors controlling hydrolysis rates (Wang et al., 2021b). Therefore, the hydrolysis lifetimes of biogenic ONs can be as fast as seconds or minutes, or as stable as several days without observable hydrolysis, depending on the structures of the ONs. Unlike bulk solutions, which only involve aqueous solutions, chamber experiments can simulate the hydrolysis of ONs formed from VOC oxidations in aerosol water. In Takeuchi and Ng (2019), the ON hydrolysis lifetimes are determined to be less than 30 minutes for NO_3 oxidation and OH-initiated photooxidation of α-pinene and β-pinene systems. The hydrolysis lifetime of ONs formed from OH-initiated photooxidation of β-ocimene has been found to be pH-dependent, 51 (±13) minutes at a pH of 4 and 24 (±3) minutes at a pH of 2.5 (Morales et al., 2021).

There is limited study on the hydrolysis of anthropogenic ONs. Only one study reported the hydrolysis lifetime of ONs resulting from OH-initiated photooxidation of 1,2,4-trimethylbenzene to be 6 hours (Liu et al., 2012). The extended hydrolysis lifetime of ONs from this system can be explained by the cleavage of the benzene ring, which disrupts the delocalized π orbitals. In this study, we determine that the hydrolysis lifetime for ONs from styrene+NO_3 oxidation is less than 30 minutes. Based on our previous work with bulk solutions (Wang et al., 2021b), we propose that the benzene-related skeleton of aromatic ONs, which contains three delocalized π orbitals, can lead to rapid hydrolysis. This is because the delocalized π orbitals enhance the hyperconjugation effect and stabilize the carbocation, thereby decrease the hydrolysis lifetimes of ONs (Wang et al., 2021b). This mechanism helps explain the short hydrolysis lifetimes observed in this work.

The fraction of hydrolyzable ONs is crucial for understanding the role of hydrolysis as a loss mechanism for ONs and NO_x. Takeuchi and Ng (2019) reported that the hydrolysable fraction of ONs from the NO_3 oxidation and OH-initiated photooxidation of α-pinene and β-pinene systems range from 9-36%. However, more than 50% of the ONs resulting from the OH-initiated photooxidation of 1,2,4-trimethylbenzene are hydrolyzable (Liu et al., 2012). In our study, we observe that the fraction of hydrolyzed styrene-derived ONs ranges from 52.7% to 60.6%. Overall, while research on the fraction of hydrolyzable ONs is still limited, these findings so far indicate that the hydrolyzable fraction of ONs resulting from the oxidation of aromatic VOCs are larger than those from biogenic VOCs. The difference can likely be explained by the fact that only ONs with specific chemical structures, particularly tertiary nitrates in biogenic VOCs oxidation systems, are susceptible to hydrolysis. In contrast, a large fraction of

410   aromatic ONs features structures with delocalized π orbitals, which facilitate hydrolysis.

411   **5.   Atmospheric implications**

412   To the best of our knowledge, this study is the first to demonstrate the formation of SOA and particulate

413   ONs from styrene+NO_3 oxidation. We systematically carry out a series of chamber experiments with initial

414   styrene concentrations ranging from 9.5 to 155.2 ppb under dry and humid conditions at room temperature.

415   The resulting SOA yields range from 4.5% to 16.1% with the aerosol mass loadings of 1.9 to 107.4 µg/m³.

416   It is known that the loss of organic vapors to the chamber wall can lead to underestimation of SOA yields.

417   For instance, Zhang et al. (2014) compare the results from a statistical oxidation model and experimental

418   observations and determine that the correction factor for SOA yields to range from 2.1 to 4.2. Here, we use

419   a semi-empirical model that incorporates the gas-to-particle partitioning of two semi-volatile products to

420   correct for the effect of vapor wall loss on SOA yields, the correction factor is found to range from 1.3 to

421   3.2, consistent with previous studies (Zhang et al., 2014). By applying the correction factor derived in this

422   work, the corrected SOA yields range from 14.0% to 22.1% with the aerosol mass loadings of 5.9 to 147.6

423   µg/m³. The yields obtained in this study provide the basis to determine the contributions of styrene+NO_3

424   chemistry to SOA formation. Styrene has been detected at the ppb levels in ambient atmosphere and has a

425   high emission factor from biomass burning, with typical abundance ranging from 0.06 to 45 ppb (Cho et

426   al., 2014; Tuazon et al., 1993; Yu et al., 2019; Koss et al., 2018). These are in the range of our experiments,

427   corresponding to the formation of up to 32.5 µg/m³ of SOA with the vapor wall loss correction. Our results

428   serve as fundamental inputs for parameterizing SOA formation from styrene in atmospheric models.

429   We examine the chemical composition of SOA and propose formation mechanisms for the major

430   monomeric and dimeric ON products detected in the particle phase. We find that dimeric products constitute

431   90.9% of the signal, while monomeric products account for only 9.1%. Previous studies have suggested

432   nitrogen-containing products measured in ambient environments are nitroaromatic compounds ($R-NO_2$)

433   formed from aromatic VOCs (Kong et al., 2021; Wang et al., 2021a; Salvador et al., 2021). Our work

434   introduces an alternative perspective, suggesting that ONs could also be nitrogen-containing products from

435   the oxidation of aromatic VOCs in the atmosphere. Dimeric nitrogen-containing compounds from the

436   oxidation of aromatic VOCs (*e.g.*, toluene, p-xylene, ethylbenzene, 1,3,5-trimethylbenzene, phenol, cresol,

437   2,6-dimethylphenol, and etc.) have been observed in chamber experiments (Molteni et al., 2018; Kumar et

438   al., 2023; Mayorga et al., 2021). Here, based on speciated molecular level characterization of SOA, we are

439   able to propose the chemical structures and formation mechanisms of dimeric ON products for the first

440   time. Besides the common RO_2+RO_2 pathway, we also suggest that other radical chain termination reactions,

441   such as RO+R or R+R, could explain the formation of the major dimeric ONs. Further density functional

442   theory calculations and experimental work are needed to provide additional evidence for confirming the

443   molecular structures and identifying critical intermediates to validate our proposed mechanisms. In contrast

444   to chamber experiments, the detection of dimeric nitrogen-containing compounds derived from aromatics

445   is rare in field campaigns. Ye et al. (2021) observe $C_{\geq 19}H_yO_zN_{1-2}$ compounds in ambient aerosols in

446   Shenzhen, China by FIGAERO-CIMS, exhibiting a ring and double-bond equivalence (RDBE) exceeding

447   10 and an aromaticity equivalent (Xc) surpassing 2.70 (Yassine et al., 2014; Wang et al., 2017). These

448   compounds can be considered as aromatic ONs (Table S3). Considering the difference between controlled

449   laboratory experiments and the complexity of ambient environments, it will be intriguing to explore why

450   dimeric ONs derived from aromatic compounds are rarely observed in the field.

451   In this study, we observe that the hydrolysis lifetime of styrene-derived ONs (about 52.7 to 60.6% of

452   total ONs) is less than 30 minutes. This finding supports our previous assumptions about the relationship

453   between hydrolysis lifetimes and the molecular structures of ONs (Wang et al., 2021b). The unique

454   delocalized π orbitals provided by the benzene-related skeleton of styrene ONs can stabilize the carbocation,

455   thereby promoting hydrolysis. The hydrolysis lifetime observed for ONs generated from styrene+NO_3

456   oxidation can serve as experimentally constrained parameter for modeling hydrolysis of aromatic ONs in

457   general. For example, not only styrene-derived ONs but also other aromatic ONs such as furan or

458   methylfuran ONs (Joo et al., 2019), despite lacking benzene ring, have the potential to undergo rapid

459   hydrolysis due to the presence of delocalized π orbitals. The hydrolysis lifetimes are crucial for regional

460   and global chemical transport models to accurately assess the impacts of hydrolysis of aromatic ONs on the

461   nitrogen budget and subsequent ozone formation.

462

463   **Data availability.**

464   The chamber experiment data are available online at the Index of Chamber Atmospheric Research in the

465   United States (ICARUS, https://icarus.ucdavis.edu/).

466

467   **Supporting Information**

468   The Supporting Information is available free of charge at: https:// /acp.copernicus.org. Additional details

469   on volatility calibration, HR-ToF-AMS and FIGAERO-CIMS mass spectra of SOA from styrene+NO_3

470   oxidation, representative product distribution, time series data from HR-ToF-AMS for different RH

471   experiments, literature review of previous styrene oxidation studies, method for correcting vapor wall loss

472   when determining SOA yields, and other proposed mechanisms for the major particle-phase products.

473

474   **Author contributions**

475   YW and NLN designed the research. YW conducted the experiments. YW, XZ, and NLN interpreted the

476   data and wrote the paper. YL conducted volatility calibration and YH helped with vapor wall loss correction.

477   All the authors discussed the results and commented on the paper.

478

479   **Competing interests.**

480   The authors declare that they have no conflict of interest.

481

482   **Acknowledgements**

483   The authors would like to acknowledge financial support by the Young Scientists Fund of the National

484   Nature Science Foundation of China (Grants 22306059), the National Science Foundation (NSF) CAREER

485   AGS-1555034 and the National Oceanic and Atmospheric Administration (NOAA) NA18OAR4310112.

486   This work was also supported by the Science and Technology Innovation Program of Hunan Province

487   (Grants 2024RC3106), the Science and Technology Planning Project of Hunan Province (Grants

488   2023JJ40128), the Nature Science Foundation of Changsha (Grant kq2208019), the Fundamental Research

489   Funds for the Central Universities (Grant 531118010830), and State Key Laboratory of Loess and

490   Quaternary Geology, Institute of Earth Environment (Grant SKLLQG2235). The FIGAERO-CIMS was

491   purchased through NSF Major Research Instrumentation (MRI) grant 1428738. The authors would also like

492   to acknowledge Dr. Long Jia for kindly providing the raw data in his paper (Yu et al., 2022a) for Figure S6.

493

494   **References:**

495   Alfarra, M. R., Paulsen, D., Gysel, M., Garforth, A. A., Dommen, J., Prévôt, A. S. H., Worsnop, D. R.,

496   Baltensperger, U., and Coe, H.: A mass spectrometric study of secondary organic aerosols formed

497   from the photooxidation of anthropogenic and biogenic precursors in a reaction chamber, Atmos.

498   Chem. Phys., 6, 5279–5293, https://doi.org/10.5194/acp-6-5279-2006, 2006.

499   Atkinson, R. and Aschmann, S. M.: Kinetics of the reactions of acenaphthene and acenaphthylene and

500   structurally-related aromatic compounds with OH and NO3 radicals, N2O5 and O3 at 296 ± 2 K, Int.

501   J. Chem. Kinet., 20, 513–539, https://doi.org/10.1002/kin.550200703, 1988.

502   Bahreini, R., Keywood, M. D., Ng, N. L., Varutbangkul, V., Gao, S., Flagan, R. C., Seinfeld, J. H., Worsnop,

503   D. R., and Jimenez, J. L.: Measurements of secondary organic aerosol from oxidation of cycloalkenes,

504   terpenes, and m-xylene using an aerodyne aerosol mass spectrometer, Environ. Sci. Technol., 39,

505   5674–5688, https://doi.org/10.1021/es048061a, 2005.

506   Boyd, C. M., Sanchez, J., Xu, L., Eugene, A. J., Nah, T., Tuet, W. Y., Guzman, M. I., and Ng, N. L.:

507   Secondary organic aerosol formation from the β-pinene+NO3 system: Effect of humidity and peroxy

508   radical fate, Atmos. Chem. Phys., 15, 7497–7522, https://doi.org/10.5194/acp-15-7497-2015, 2015.

509   Boyd, C. M., Nah, T., Xu, L., Berkemeier, T., and Ng, N. L.: Secondary Organic Aerosol (SOA) from

510   Nitrate Radical Oxidation of Monoterpenes: Effects of Temperature, Dilution, and Humidity on

Aerosol Formation, Mixing, and Evaporation, Environ. Sci. Technol., 51, 7831–7841, https://doi.org/10.1021/acs.est.7b01460, 2017.

Cabrera-Perez, D., Taraborrelli, D., Sander, R., and Pozzer, A.: Global atmospheric budget of simple monocyclic aromatic compounds, Atmos. Chem. Phys., 16, 6931–6947, https://doi.org/10.5194/acp-16-6931-2016, 2016.

Calvert, J. G., Atkinson, R., Becker, K. H., Kamens, R. M., Seinfeld, J. H., Wallington, T. H., and Yarwood, G.: The Mechanisms of Atmospheric Oxidation of the Aromatic Hydrocarbons, Oxford University Press, 2002.

Canagaratna, M. R., Jimenez, J. L., Kroll, J. H., Chen, Q., Kessler, S. H., Massoli, P., Hildebrandt Ruiz, L., Fortner, E., Williams, L. R., Wilson, K. R., Surratt, J. D., Donahue, N. M., Jayne, J. T., and Worsnop, D. R.: Elemental ratio measurements of organic compounds using aerosol mass spectrometry: Characterization, improved calibration, and implications, Atmos. Chem. Phys., 15, 253–272, https://doi.org/10.5194/acp-15-253-2015, 2015.

Chen, T., Chu, B., Ma, Q., Zhang, P., Liu, J., and He, H.: Effect of relative humidity on SOA formation from aromatic hydrocarbons: Implications from the evolution of gas- and particle-phase species, Sci. Total Environ., 773, 145015, https://doi.org/10.1016/j.scitotenv.2021.145015, 2021.

Chen, Y., Takeuchi, M., Nah, T., Xu, L., Canagaratna, M. R., Stark, H., Baumann, K., Canonaco, F., Prevot, A. S. H., Gregory Huey, L., Weber, R. J., and Ng, N. L.: Chemical characterization of secondary organic aerosol at a rural site in the southeastern US: Insights from simultaneous high-resolution time-of-flight aerosol mass spectrometer (HR-ToF-AMS) and FIGAERO chemical ionization mass spectrometer (CIMS) measur, Atmos. Chem. Phys., 20, 8421–8440, https://doi.org/10.5194/acp-20-8421-2020, 2020.

Cho, J., Roueintan, M., and Li, Z.: Kinetic and dynamic investigations of oh reaction with styrene, J. Phys. Chem. A, 118, 9460–9470, https://doi.org/10.1021/jp501380j, 2014.

Darer, A. I., Cole-Filipiak, N. C., O'Connor, A. E., and Elrod, M. J.: Formation and stability of atmospherically relevant isoprene-derived organosulfates and organonitrates, Environ. Sci. Technol., 45, 1895–1902, https://doi.org/10.1021/es103797z, 2011.

Day, D. A., Campuzano-jost, P., Nault, B. A., Palm, B. B., Hu, W., Martin, S. T., and Jimenez, J. L.: A systematic re-evaluation of methods for quantification of bulk particle-phase organic nitrates using real-time aerosol mass spectrometry, Atmos. Meas. Tech., 15, 459–483, 2022.

DeCarlo, P. F., Kimmel, J. R., Trimborn, A., Northway, M. J., Jayne, J. T., Aiken, A. C., Gonin, M., Fuhrer, K., Horvath, T., Docherty, K. S., Worsnop, D. R., and Jimenez, J. L.: Field-deployable, high-resolution, time-of-flight aerosol mass spectrometer, Anal. Chem., 78, 8281–8289, https://doi.org/10.1021/ac061249n, 2006.

545   Decker, Z. C. J., Robinson, M. A., Barsanti, K. C., Bourgeois, I., Coggon, M. M., Digangi, J. P., Diskin, G.
546   S., Flocke, F. M., Franchin, A., Fredrickson, C. D., Gkatzelis, G. I., Hall, S. R., Halliday, H., Holmes,
547   C. D., Huey, L. G., Lee, Y. R., Lindaas, J., Middlebrook, A. M., Montzka, D. D., Moore, R., Neuman,
548   J. A., Nowak, J. B., Palm, B. B., Peischl, J., Piel, F., Rickly, P. S., Rollins, A. W., Ryerson, T. B.,
549   Schwantes, R. H., Sekimoto, K., Thornhill, L., Thornton, J. A., Tyndall, G. S., Ullmann, K., Van Rooy,
550   P., Veres, P. R., Warneke, C., Washenfelder, R. A., Weinheimer, A. J., Wiggins, E., Winstead, E.,
551   Wisthaler, A., Womack, C., and Brown, S. S.: Nighttime and daytime dark oxidation chemistry in
552   wildfire plumes: An observation and model analysis of FIREX-AQ aircraft data, Atmos. Chem. Phys.,
553   21, 16293–16317, https://doi.org/10.5194/acp-21-16293-2021, 2021.
554   Farmer, D. K., Matsunaga, A., Docherty, K. S., Surratt, J. D., Seinfeld, J. H., Ziemann, P. J., and Jimenez,
555   J. L.: Response of an aerosol mass spectrometer to organonitrates and organosulfates and implications
556   for atmospheric chemistry, Proc. Natl. Acad. Sci. U. S. A., 107, 6670–6675,
557   https://doi.org/10.1073/pnas.0912340107, 2010.
558   Fisher, J. A., Jacob, D. J., Travis, K. R., Kim, P. S., Marais, E. A., Miller, C. C., Yu, K., Zhu, L., Yantosca,
559   R. M., Sulprizio, M. P., Mao, J., Wennberg, P. O., Crounse, J. D., Teng, A. P., Nguyen, T. B., Clair,
560   J. M. S., Cohen, R. C., Romer, P., Nault, B. A., Wooldridge, P. J., Jimenez, J. L., Campuzano-Jost, P.,
561   Day, D. A., Hu, W., Shepson, P. B., Xiong, F., Blake, D. R., Goldstein, A. H., Misztal, P. K., Hanisco,
562   T. F., Wolfe, G. M., Ryerson, T. B., Wisthaler, A., and Mikoviny, T.: Organic nitrate chemistry and
563   its implications for nitrogen budgets in an isoprene- and monoterpene-rich atmosphere: Constraints
564   from aircraft (SEAC4RS) and ground-based (SOAS) observations in the Southeast US, 5969–5991
565   pp., https://doi.org/10.5194/acp-16-5969-2016, 2016.
566   Frka, S., Šala, M., Kroflič, A., Huš, M., Čusak, A., and Grgić, I.: Quantum Chemical Calculations Resolved
567   Identification of Methylnitrocatechols in Atmospheric Aerosols, Environ. Sci. Technol., 50, 5526–
568   5535, https://doi.org/10.1021/acs.est.6b00823, 2016.
569   Grosjean, D.: Wall Loss of Gaseous Pollutants in Outdoor Teflon Chambers, Environ. Sci. Technol., 19,
570   1059–1065, https://doi.org/10.1021/es00141a006, 1985.
571   Helal, S. F. and Elshafy, W. S.: Health hazards among workers in plastic industry, Toxicol. Ind. Health, 29,
572   812–819, https://doi.org/10.1177/0748233712442728, 2012.
573   Henry, K. M. and Donahue, N. M.: Photochemical aging of α-pinene secondary organic aerosol: Effects of
574   OH radical sources and photolysis, J. Phys. Chem. A, 116, 5932–5940,
575   https://doi.org/10.1021/jp210288s, 2012.
576   Hu, K. S., Darer, A. I., and Elrod, M. J.: Thermodynamics and kinetics of the hydrolysis of atmospherically
577   relevant organonitrates and organosulfates, Atmos. Chem. Phys., 11, 8307–8320,
578   https://doi.org/10.5194/acp-11-8307-2011, 2011.

579 Huang, Y., Zhao, R., Charan, S. M., Kenseth, C. M., Zhang, X., and Seinfeld, J. H.: Unified Theory of
580   Vapor-Wall Mass Transport in Teflon-Walled Environmental Chambers, Environ. Sci. Technol., 52,
581   2134–2142, https://doi.org/10.1021/acs.est.7b05575, 2018.

582 Jacobs, M. I., Burke, W. J., and Elrod, M. J.: Kinetics of the reactions of isoprene-derived hydroxynitrates:
583   Gas phase epoxide formation and solution phase hydrolysis, Atmos. Chem. Phys., 14, 8933–8946,
584   https://doi.org/10.5194/acp-14-8933-2014, 2014.

585 Jenkin, M. E., Saunders, S. M., Wagner, V., and Pilling, M. J.: Protocol for the development of the Master
586   Chemical Mechanism, MCM v3 (Part B): Tropospheric degradation of aromatic volatile organic
587   compounds, Atmos. Chem. Phys., 3, 181–193, https://doi.org/10.5194/acp-3-181-2003, 2003.

588 Jiang, H., Cai, J., Feng, X., Chen, Y., Wang, L., Jiang, B., Liao, Y., Li, J., Zhang, G., Mu, Y., and Chen, J.:
589   Aqueous-Phase Reactions of Anthropogenic Emissions Lead to the High Chemodiversity of
590   Atmospheric Nitrogen-Containing Compounds during the Haze Event, Environ. Sci. Technol., 57,
591   16500–16511, https://doi.org/10.1021/acs.est.3c06648, 2023.

592 Joo, T., Rivera-Rios, J. C., Takeuchi, M., Alvarado, M. J., and Ng, N. L.: Secondary Organic Aerosol
593   Formation from Reaction of 3-Methylfuran with Nitrate Radicals, ACS Earth Sp. Chem., 3, 922–934,
594   https://doi.org/10.1021/acsearthspacechem.9b00068, 2019.

595 Kinney, P. D., Pui, D. Y. H., Mulholland, G. W., and Bryner, N. P.: Use of the electrostatic classification
596   method to size 0.1 micrometer SRM particles - A feasibility study, J. Res. Natl. Inst. Stand. Technol.,
597   96, 147, https://doi.org/10.6028/jres.096.006, 1991.

598 Knighton, W. B., Herndon, S. C., Wood, E. C., Fortner, E. C., Onasch, T. B., Wormhoudt, J., Kolb, C. E.,
599   Lee, B. H., Zavala, M., Molina, L., and Jones, M.: Detecting fugitive emissions of 1,3-butadiene and
600   styrene from a petrochemical facility: An application of a mobile laboratory and a modified proton
601   transfer reaction mass spectrometer, Ind. Eng. Chem. Res., 51, 12706–12711,
602   https://doi.org/10.1021/ie202794j, 2012.

603 Kong, X., Salvador, C. M., Carlsson, S., Pathak, R., Davidsson, K. O., Le Breton, M., Gaita, S. M., Mitra,
604   K., Hallquist, Å. M., Hallquist, M., and Pettersson, J. B. C.: Molecular characterization and optical
605   properties of primary emissions from a residential wood burning boiler, Sci. Total Environ., 754,
606   142143, https://doi.org/10.1016/j.scitotenv.2020.142143, 2021.

607 Koss, A. R., Sekimoto, K., Gilman, J. B., Selimovic, V., Coggon, M. M., Zarzana, K. J., Yuan, B., Lerner,
608   B. M., Brown, S. S., Jimenez, J. L., Krechmer, J., Roberts, J. M., Warneke, C., Yokelson, R. J., and
609   De Gouw, J.: Non-methane organic gas emissions from biomass burning: Identification, quantification,
610   and emission factors from PTR-ToF during the FIREX 2016 laboratory experiment, Atmos. Chem.
611   Phys., 18, 3299–3319, https://doi.org/10.5194/acp-18-3299-2018, 2018.

612 Krechmer, J. E., Pagonis, D., Ziemann, P. J., and Jimenez, J. L.: Quantification of Gas-Wall Partitioning in

Teflon Environmental Chambers Using Rapid Bursts of Low-Volatility Oxidized Species Generated in Situ, Environ. Sci. Technol., 50, 5757–5765, https://doi.org/10.1021/acs.est.6b00606, 2016.

Kumar, V., Slowik, J. G., Baltensperger, U., Prevot, A. S. H., and Bell, D. M.: Time-Resolved Molecular Characterization of Secondary Organic Aerosol Formed from OH and NO3 Radical Initiated Oxidation of a Mixture of Aromatic Precursors, Environ. Sci. Technol., 57, 11572–11582, https://doi.org/10.1021/acs.est.3c00225, 2023.

La, Y. S., Camredon, M., Ziemann, P. J., Valorso, R., Matsunaga, A., Lannuque, V., Lee-Taylor, J., Hodzic, A., Madronich, S., and Aumont, B.: Impact of chamber wall loss of gaseous organic compounds on secondary organic aerosol formation: Explicit modeling of SOA formation from alkane and alkene oxidation, Atmos. Chem. Phys., 16, 1417–1431, https://doi.org/10.5194/acp-16-1417-2016, 2016.

Lee, B. H., Mohr, C., Lopez-Hilfiker, F. D., Lutz, A., Hallquist, M., Lee, L., Romer, P., Cohen, R. C., Iyer, S., Kurtén, T., Hu, W., Day, D. A., Campuzano-Jost, P., Jimenez, J. L., Xu, L., Ng, N. L., Guo, H., Weber, R. J., Wild, R. J., Brown, S. S., Koss, A., Gouw, J. de, Olson, K., Goldstein, A. H., Seco, R., Kim, S., McAvey, K., Shepson, P. B., Starn, T., Baumann, K., Edgerton, E. S., Liu, J., Shilling, J. E., Miller, D. O., Brune, W., Schobesberger, S., D'Ambro, E. L., and Thornton, J. A.: Highly functionalized organic nitrates in the southeast United States: Contribution to secondary organic aerosol and reactive nitrogen budgets, Proc. Natl. Acad. Sci., 113, 1516–1521, https://doi.org/10.1073/PNAS.1508108113, 2016.

Lewis, R. J. and Moodie, R. B.: Nitration of styrenes by dinitrogen pentoxide in dichloromethane, J. Chem. Soc. Perkin Trans. 2, 1315–1320, 1996.

Lin, C., Huang, R. J., Duan, J., Zhong, H., and Xu, W.: Primary and Secondary Organic Nitrate in Northwest China: A Case Study, Environ. Sci. Technol. Lett., 8, 947–953, https://doi.org/10.1021/acs.estlett.1c00692, 2021.

Liu, S., Shilling, J. E., Song, C., Hiranuma, N., Zaveri, R. A., and Russell, L. M.: Hydrolysis of organonitrate functional groups in aerosol particles, Aerosol Sci. Technol., 46, 1359–1369, https://doi.org/10.1080/02786826.2012.716175, 2012.

Liu, S., Liu, X., Wang, Y., Zhang, S., Wu, C., Du, W., and Wang, G.: Effect of NOx and RH on the secondary organic aerosol formation from toluene photooxidation, J. Environ. Sci. (China), 114, 1–9, https://doi.org/10.1016/j.jes.2021.06.017, 2022.

Lopez-Hilfiker, F. D., Mohr, C., Ehn, M., Rubach, F., Kleist, E., Wildt, J., Mentel, T. F., Lutz, A., Hallquist, M., Worsnop, D., and Thornton, J. A.: A novel method for online analysis of gas and particle composition: Description and evaluation of a filter inlet for gases and AEROsols (FIGAERO), Atmos. Meas. Tech., 7, 983–1001, https://doi.org/10.5194/amt-7-983-2014, 2014.

Lopez-Hilfiker, F. D., Mohr, C., D'Ambro, E. L., Lutz, A., Riedel, T. P., Gaston, C. J., Iyer, S., Zhang, Z.,

647 Gold, A., Surratt, J. D., Lee, B. H., Kurten, T., Hu, W. W., Jimenez, J., Hallquist, M., and Thornton,

648 J. A.: Molecular Composition and Volatility of Organic Aerosol in the Southeastern U.S.: Implications

649 for IEPOX Derived SOA, Environ. Sci. Technol., 50, 2200–2209,

650 https://doi.org/10.1021/acs.est.5b04769, 2016.

651 Lu, B., Meng, X., Dong, S., Zhang, Z., Liu, C., Jiang, J., Herrmann, H., and Li, X.: High-resolution mapping

652 of regional VOCs using the enhanced space-time extreme gradient boosting machine (XGBoost) in

653 Shanghai, Sci. Total Environ., 905, 167054, https://doi.org/10.1016/j.scitotenv.2023.167054, 2023a.

654 Lu, Y., Ma, Y., Huang, D. D., Lou, S., Jing, S., Gao, Y., Wang, H., Zhang, Y., Chen, H., Chang, Y., Yan,

655 N., Chen, J., George, C., Riva, M., and Huang, C.: Unambiguous identification of N-containing

656 oxygenated organic molecules using a chemical-ionization Orbitrap (CI-Orbitrap) in an eastern

657 Chinese megacity, Atmos. Chem. Phys., 23, 3233–3245, https://doi.org/10.5194/acp-23-3233-2023,

658 2023b.

659 Ma, Q., Lin, X., Yang, C., Long, B., Gai, Y., and Zhang, W.: The influences of ammonia on aerosol

660 formation in the ozonolysis of styrene: Roles of criegee intermediate reactions, R. Soc. Open Sci., 5,

661 172171–172183, https://doi.org/10.1098/rsos.172171, 2018.

662 Matsunaga, A. and Ziemann, P. J.: Gas-wall partitioning of organic compounds in a teflon film chamber

663 and potential effects on reaction product and aerosol yield measurements, Aerosol Sci. Technol., 44,

664 881–892, https://doi.org/10.1080/02786826.2010.501044, 2010.

665 Mayorga, R. J., Zhao, Z., and Zhang, H.: Formation of secondary organic aerosol from nitrate radical

666 oxidation of phenolic VOCs: Implications for nitration mechanisms and brown carbon formation,

667 Atmos. Environ., 244, 117910, https://doi.org/10.1016/j.atmosenv.2020.117910, 2021.

668 McLafferty, F. W. and Turecek, F.: Interpretation Of Mass Spectra, University Science Books, 1993.

669 McMurry, J.: Organic Chemistry, Brooks/Cole Cengage Learning, 2012.

670 McMurry, P. H. and Grosjean, D.: Gas and Aerosol Wall Losses in Teflon Film Smog Chambers, Environ.

671 Sci. Technol., 19, 1176–1182, https://doi.org/10.1021/es00142a006, 1985.

672 Molteni, U., Bianchi, F., Klein, F., El Haddad, I., Frege, C., Rossi, M. J., Dommen, J., and Baltensperger,

673 U.: Formation of highly oxygenated organic molecules from aromatic compounds, Atmos. Chem.

674 Phys., 18, 1909–1921, https://doi.org/10.5194/acp-18-1909-2018, 2018.

675 Morales, A. C., Jayarathne, T., Slade, J. H., Laskin, A., and Shepson, P. B.: The production and hydrolysis

676 of organic nitrates from OH radical oxidation of β-ocimene, Atmos. Chem. Phys., 21, 129–145,

677 https://doi.org/10.5194/acp-21-129-2021, 2021.

678 Na, K., Song, C., and Cocker, D. R.: Formation of secondary organic aerosol from the reaction of styrene

679 with ozone in the presence and absence of ammonia and water, Atmos. Environ., 40, 1889–1900,

680 https://doi.org/10.1016/j.atmosenv.2005.10.063, 2006.

681 Nah, T., Mcvay, R. C., Zhang, X., Boyd, C. M., Seinfeld, J. H., and Ng, N. L.: Influence of seed aerosol

682   surface area and oxidation rate on vapor wall deposition and SOA mass yields : a case study with α -

683   pinene ozonolysis, Atmos. Chem. Phys., 16, 9361–9379, https://doi.org/10.5194/acp-16-9361-2016,

684   2016a.

685 Nah, T., Sanchez, J., Boyd, C. M., and Ng, N. L.: Photochemical Aging of α-pinene and β-pinene Secondary

686   Organic Aerosol formed from Nitrate Radical Oxidation, Environ. Sci. Technol., 50, 222–231,

687   https://doi.org/10.1021/acs.est.5b04594, 2016b.

688 Nah, T., McVay, R. C., Pierce, J. R., Seinfeld, J. H., and Ng, N. L.: Constraining uncertainties in particle-

689   wall deposition correction during SOA formation in chamber experiments, Atmos. Chem. Phys., 17,

690   2297–2310, https://doi.org/10.5194/acp-17-2297-2017, 2017.

691 Ng, L. N., Brown, S. S., Archibald, A. T., Atlas, E., Cohen, R. C., Crowley, J. N., Day, D. A., Donahue, N.

692   M., Fry, J. L., Fuchs, H., Griffin, R. J., Guzman, M. I., Herrmann, H., Hodzic, A., Iinuma, Y., Kiendler-

693   Scharr, A., Lee, B. H., Luecken, D. J., Mao, J., McLaren, R., Mutzel, A., Osthoff, H. D., Ouyang, B.,

694   Picquet-Varrault, B., Platt, U., Pye, H. O. T., Rudich, Y., Schwantes, R. H., Shiraiwa, M., Stutz, J.,

695   Thornton, J. A., Tilgner, A., Williams, B. J., and Zaveri, R. A.: Nitrate radicals and biogenic volatile

696   organic compounds: Oxidation, mechanisms, and organic aerosol, Atmos. Chem. Phys., 17, 2103–

697   2162, https://doi.org/10.5194/acp-17-2103-2017, 2017.

698 Ng, N. L., Kwan, A. J., Surratt, J. D., Chan, A. W. H., Chhabra, P. S., Sorooshian, A., Pye, H. O. T., Crounse,

699   J. D., Wennberg, P. O., Flagan, R. C., and Seinfeld, J. H.: Secondary organic aerosol (SOA) formation

700   from reaction of isoprene with nitrate radicals (NO3), Atmos. Chem. Phys., 8, 4117–4140,

701   https://doi.org/10.5194/acp-8-4117-2008, 2008.

702 Odum, J. R., Hoffmann, T., Bowman, F., Collins, D., Flagan, R. C., and Seinfeld, J. H.: Gas/particle

703   partitioning and secondary organic aerosol yields, Environ. Sci. Technol., 30, 2580–2585,

704   https://doi.org/10.1021/es950943+, 1996.

705 Odum, J. R., Jungkamp, T. P. W., Griffin, R. J., Flagan, R. C., and Seinfeld, J. H.: The Atmospheric

706   Aerosol-Forming Potential of Whole Gasoline Vapor, Science (80-.)., 276, 96–99,

707   https://doi.org/10.1126/science.276.5309.96, 1997.

708 Okada, Y., Nakagoshi, A., Tsurukawa, M., Matsumura, C., Eiho, J., and Nakano, T.: Environmental risk

709   assessment and concentration trend of atmospheric volatile organic compounds in Hyogo Prefecture,

710   Japan, Environ. Sci. Pollut. Res., 19, 201–213, https://doi.org/10.1007/s11356-011-0550-0, 2012.

711 Orel, A. E., Peterson, T. W., and Seinfeld, J. H.: Nitrate Formation in Atmospheric Aerosols., Environ. Sci.

712   Technol., 18, 410–411, https://doi.org/10.1021/es60142a016, 1978.

713 Le Person, A., Eyglunent, G., Daële, V., Mellouki, A., and Mu, Y.: The near UV absorption cross-sections

714   and the rate coefficients for the ozonolysis of a series of styrene-like compounds, J. Photochem.

715   Photobiol. A Chem., 195, 54–63, https://doi.org/10.1016/j.jphotochem.2007.09.006, 2008.

716   Pye, H. O. T., Luecken, D. J., Xu, L., Boyd, C. M., Ng, N. L., Baker, K. R., Ayres, B. R., Bash, J. O.,

717   Baumann, K., Carter, W. P. L., Edgerton, E., Fry, J. L., Hutzell, W. T., Schwede, D. B., and Shepson,

718   P. B.: Modeling the Current and Future Roles of Particulate Organic Nitrates in the Southeastern

719   United States, Environ. Sci. Technol., 49, 14195–14203, https://doi.org/10.1021/acs.est.5b03738,

720   2015.

721   Rindelaub, J. D., Borca, C. H., Hostetler, M. A., Slade, J. H., Lipton, M. A., Slipchenko, L. V., and Shepson,

722   P. B.: The acid-catalyzed hydrolysis of an α-pinene-derived organic nitrate: Kinetics, products,

723   reaction mechanisms, and atmospheric impact, Atmos. Chem. Phys., 16, 15425–15432,

724   https://doi.org/10.5194/acp-16-15425-2016, 2016.

725   Salvador, C. M. G., Tang, R., Priestley, M., Li, L., Tsiligiannis, E., Le Breton, M., Zhu, W., Zeng, L., Wang,

726   H., Yu, Y., Hu, M., Guo, S., and Hallquist, M.: Ambient nitro-aromatic compounds-biomass burning

727   versus secondary formation in rural China, Atmos. Chem. Phys., 21, 1389–1406,

728   https://doi.org/10.5194/acp-21-1389-2021, 2021.

729   Schueneman, M. K., Day, D. A., Peng, Z., Pagonis, D., Jenks, O. J., de Gouw, J. A., and Jimenez, J. L.:

730   Secondary Organic Aerosol Formation from the OH Oxidation of Phenol, Catechol, Styrene, Furfural,

731   and Methyl Furfural, ACS Earth Sp. Chem., 8, 1179–1192,

732   https://doi.org/10.1021/acsearthspacechem.3c00361, 2024.

733   Stark, H., Yatavelli, R. L. N., Thompson, S. L., Kang, H., Krechmer, J. E., Kimmel, J. R., Palm, B. B., Hu,

734   W., Hayes, P. L., Day, D. A., Campuzano-Jost, P., Canagaratna, M. R., Jayne, J. T., Worsnop, D. R.,

735   and Jimenez, J. L.: Impact of Thermal Decomposition on Thermal Desorption Instruments: Advantage

736   of Thermogram Analysis for Quantifying Volatility Distributions of Organic Species, Environ. Sci.

737   Technol., 51, 8491–8500, https://doi.org/10.1021/acs.est.7b00160, 2017.

738   Sun, J., Wu, F., Hu, B., Tang, G., Zhang, J., and Wang, Y.: VOC characteristics, emissions and

739   contributions to SOA formation during hazy episodes, Atmos. Environ., 141, 560–570,

740   https://doi.org/10.1016/j.atmosenv.2016.06.060, 2016.

741   Tajuelo, M., Bravo, I., Rodríguez, A., Aranda, A., Díaz-de-Mera, Y., and Rodríguez, D.: Atmospheric sink

742   of styrene, A-methylstyrene, trans-B-methylstyrene and indene: Rate constants and mechanisms of Cl

743   atom-initiated degradation, Atmos. Environ., 200, 78–89,

744   https://doi.org/10.1016/j.atmosenv.2018.11.059, 2019a.

745   Tajuelo, M., Rodríguez, D., Baeza-Romero, M. T., Díaz-de-Mera, Y., Aranda, A., and Rodríguez, A.:

746   Secondary organic aerosol formation from styrene photolysis and photooxidation with hydroxyl

747   radicals, Chemosphere, 231, 276–286, https://doi.org/10.1016/j.chemosphere.2019.05.136, 2019b.

748   Takeuchi, M. and Ng, N. L.: Chemical composition and hydrolysis of organic nitrate aerosol formed from

hydroxyl and nitrate rlanadical oxidation of α-pinene and β-pinene, Atmos. Chem. Phys., 19, 12749–12766, https://doi.org/10.5194/acp-19-12749-2019, 2019.

Takeuchi, M., Berkemeier, T., Eris, G., and Ng, N. L.: Non-linear effects of secondary organic aerosol formation and properties in multi-precursor systems, Nat. Commun., 13, 1–13, https://doi.org/10.1038/s41467-022-35546-1, 2022.

Takeuchi, M., Wang, Y., Nault, B. A., Chen, Y., Canagaratna, M. R., and Ng, N. L.: Evaluating the response of the Aerodyne aerosol mass spectrometer to monoterpene- and isoprene-derived organic nitrate standards, Aerosol Sci. Technol., 0, 1–18, https://doi.org/10.1080/02786826.2024.2389183, 2024.

Tasoglou, A. and Pandis, S. N.: Formation and chemical aging of secondary organic aerosol during the β-caryophyllene oxidation, Atmos. Chem. Phys., 15, 6035–6046, https://doi.org/10.5194/acp-15-6035-2015, 2015.

Thornton, J. A., Mohr, C., Schobesberger, S., D'Ambro, E. L., Lee, B. H., and Lopez-Hilfiker, F. D.: Evaluating Organic Aerosol Sources and Evolution with a Combined Molecular Composition and Volatility Framework Using the Filter Inlet for Gases and Aerosols (FIGAERO), Acc. Chem. Res., 53, 1415–1426, https://doi.org/10.1021/acs.accounts.0c00259, 2020.

Tuazon, E. C., Arey, J., Atkinson, R., and Aschmann, S. M.: Gas-Phase Reactions of 2-Vinylpyridine and Styrene with OH and NO3 Radicals and O3, Environ. Sci. Technol., 27, 1832–1841, https://doi.org/10.1021/es00046a011, 1993.

Vasquez, K. T., Crounse, J. D., Schulze, B. C., Bates, K. H., Teng, A. P., Xu, L., Allen, H. M., and Wennberg, P. O.: Rapid hydrolysis of tertiary isoprene nitrate efficiently removes NOx from the atmosphere, Proc. Natl. Acad. Sci. U. S. A., 117, 33011–33016, https://doi.org/10.1073/PNAS.2017442117, 2021.

Vidović, K., Lašič Jurković, D., Šala, M., Kroflič, A., and Grgić, I.: Nighttime Aqueous-Phase Formation of Nitrocatechols in the Atmospheric Condensed Phase, Environ. Sci. Technol., 52, 9722–9730, https://doi.org/10.1021/acs.est.8b01161, 2018.

Vione, D., Maurino, V., Minero, C., and Pelizzetti, E.: Phenol photonitration upon UV irradiation of nitrite in aqueous solution I: Effects of oxygen and 2-propanol, Chemosphere, 45, 893–902, https://doi.org/10.1016/S0045-6535(01)00035-2, 2001.

Vione, D., Maurino, V., Minero, C., Lucchiari, M., and Pelizzetti, E.: Nitration and hydroxylation of benzene in the presence of nitrite/nitrous acid in aqueous solution, Chemosphere, 56, 1049–1059, https://doi.org/10.1016/j.chemosphere.2004.05.027, 2004.

Wang, H., Ji, Y., Gao, Y., Li, G., and An, T.: Theoretical model on the formation possibility of secondary organic aerosol from OH initialed oxidation reaction of styrene in the presence of O2/NO, Atmos. Environ., 101, 1–9, https://doi.org/10.1016/j.atmosenv.2014.10.042, 2015.

783   Wang, W., Zhang, Y., Jiang, B., Chen, Y., Song, Y., Tang, Y., Dong, C., and Cai, Z.: Molecular

784   characterization of organic aerosols in Taiyuan, China: Seasonal variation and source identification,

785   Sci. Total Environ., 800, 149419, https://doi.org/10.1016/j.scitotenv.2021.149419, 2021a.

786   Wang, X., Hayeck, N., Brüggemann, M., Yao, L., Chen, H., Zhang, C., Emmelin, C., Chen, J., George, C.,

787   and Wang, L.: Chemical Characteristics of Organic Aerosols in Shanghai: A Study by Ultrahigh-

788   Performance Liquid Chromatography Coupled With Orbitrap Mass Spectrometry, J. Geophys. Res.

789   Atmos., 122, 11,703-11,722, https://doi.org/10.1002/2017JD026930, 2017.

790   Wang, Y., Hu, M., Wang, Y., Zheng, J., Shang, D., Yang, Y., Liu, Y., Li, X., Tang, R., Zhu, W., Du, Z.,

791   Wu, Y., Guo, S., Wu, Z., Lou, S., Hallquist, M., and Yu, J. Z.: The formation of nitro-aromatic

792   compounds under high NOx and anthropogenic VOC conditions in urban Beijing, China, Atmos.

793   Chem. Phys., 19, 7649–7665, https://doi.org/10.5194/acp-19-7649-2019, 2019.

794   Wang, Y., Piletic, I. R., Takeuchi, M., Xu, T., France, S., and Ng, N. L.: Synthesis and Hydrolysis of

795   Atmospherically Relevant Monoterpene-Derived Organic Nitrates, Environ. Sci. Technol., 55, 14595–

796   14606, https://doi.org/10.1021/acs.est.1c05310, 2021b.

797   Wu, S., Tang, G., Wang, Y., Yang, Y., Yao, D., Zhao, W., Gao, W., Sun, J., and Wang, Y.: Vertically

798   decreased VOC concentration and reactivity in the planetary boundary layer in winter over the North

799   China Plain, Atmos. Res., 240, 104930, https://doi.org/10.1016/j.atmosres.2020.104930, 2020.

800   Yang, L. H., Takeuchi, M., Chen, Y., and Ng, N. L.: Characterization of thermal decomposition of

801   oxygenated organic compounds in FIGAERO-CIMS, Aerosol Sci. Technol., 55, 1321–1342,

802   https://doi.org/10.1080/02786826.2021.1945529, 2021.

803   Yang, X., Luo, F., Li, J., Chen, D., Ye, E., Lin, W., and Jin, J.: Alkyl and aromatic nitrates in atmospheric

804   particles determined by gas chromatography tandem mass spectrometry, J. Am. Soc. Mass Spectrom.,

805   30, 2762–2770, https://doi.org/10.1007/s13361-019-02347-8, 2019.

806   Yang, Y., Wang, Y., Zhou, P., Yao, D., Ji, D., Sun, J., Wang, Y., Zhao, S., Huang, W., Yang, S., Chen, D.,

807   Gao, W., Liu, Z., Hu, B., Zhang, R., Zeng, L., Ge, M., Petäjä, T., Kerminen, V. M., Kulmala, M., and

808   Wang, Y.: Atmospheric reactivity and oxidation capacity during summer at a suburban site between

809   Beijing and Tianjin, Atmos. Chem. Phys., 20, 8181–8200, https://doi.org/10.5194/acp-20-8181-2020,

810   2020.

811   Yassine, M. M., Harir, M., Dabek-Zlotorzynska, E., and Schmitt-Kopplin, P.: Structural characterization

812   of organic aerosol using Fourier transform ion cyclotron resonance mass spectrometry: aromaticity

813   equivalent approach, Rapid Commun. Mass Spectrom., 28, 2445–2454,

814   https://doi.org/10.1002/rcm.7038, 2014.

815   Ye, C., Yuan, B., Lin, Y., Wang, Z., Hu, W., Li, T., Chen, W., Wu, C., Wang, C., Huang, S., Qi, J., Wang,

816   B., Wang, C., Song, W., Wang, X., Zheng, E., Krechmer, J. E., Ye, P., Zhang, Z., Wang, X., Worsnop,

D. R., and Shao, M.: Chemical characterization of oxygenated organic compounds in the gas phase and particle phase using iodide CIMS with FIGAERO in urban air, Atmos. Chem. Phys., 21, 8455–8478, https://doi.org/10.5194/acp-21-8455-2021, 2021.

Yeh, G. K. and Ziemann, P. J.: Gas-wall partitioning of oxygenated organic compounds: Measurements, structure-activity relationships, and correlation with gas chromatographic retention factor, Aerosol Sci. Technol., 49, 727–738, https://doi.org/10.1080/02786826.2015.1068427, 2015.

Ylisirniö, A., Barreira, L. M. F., Pullinen, I., Buchholz, A., Jayne, J., Krechmer, J. E., Worsnop, D. R., Virtanen, A., and Schobesberger, S.: On the calibration of FIGAERO-ToF-CIMS: Importance and impact of calibrant delivery for the particle-phase calibration, Atmos. Meas. Tech., 14, 355–367, https://doi.org/10.5194/amt-14-355-2021, 2021.

Yu, K., Zhu, Q., Du, K., and Huang, X.: Characterization of nighttime formation of particulate organic nitrates based on high-resolution aerosol mass spectrometry in an urban atmosphere in China, Atmos. Chem. Phys., 19, 5235–5249, 2019.

Yu, L., Smith, J., Laskin, A., Anastasio, C., Laskin, J., and Zhang, Q.: Chemical characterization of SOA formed from aqueous-phase reactions of phenols with the triplet excited state of carbonyl and hydroxyl radical, Atmos. Chem. Phys., 14, 13801–13816, https://doi.org/10.5194/acp-14-13801-2014, 2014.

Yu, L., Smith, J., Laskin, A., M George, K., Anastasio, C., Laskin, J., M Dillner, A., and Zhang, Q.: Molecular transformations of phenolic SOA during photochemical aging in the aqueous phase: Competition among oligomerization, functionalization, and fragmentation, Atmos. Chem. Phys., 16, 4511–4527, https://doi.org/10.5194/acp-16-4511-2016, 2016.

Yu, S., Jia, L., Xu, Y., and Pan, Y.: Formation of extremely low-volatility organic compounds from styrene ozonolysis: Implication for nucleation, Chemosphere, 305, 135459, https://doi.org/10.1016/j.chemosphere.2022.135459, 2022a.

Yu, S. S., Jia, L., Xu, Y. F., and Pan, Y. P.: Molecular composition of secondary organic aerosol from styrene under different NOx and humidity conditions, Atmos. Res., 266, 105950, https://doi.org/10.1016/j.atmosres.2021.105950, 2022b.

Zare, A., Fahey, K. M., Sarwar, G., Cohen, R. C., and Pye, H. O. T.: Vapor-Pressure Pathways Initiate but Hydrolysis Products Dominate the Aerosol Estimated from Organic Nitrates, ACS Earth Sp. Chem., 3, 1426–1437, https://doi.org/10.1021/acsearthspacechem.9b00067, 2019.

Zhang, X., Cappa, C. D., Jathar, S. H., McVay, R. C., Ensberg, J. J., Kleeman, M. J., and Seinfeld, J. H.: Influence of vapor wall loss in laboratory chambers on yields of secondary organic aerosol, Proc. Natl. Acad. Sci. U. S. A., 111, 5802–5807, https://doi.org/10.1073/pnas.1404727111, 2014.

Zhang, X., Schwantes, R. H., McVay, R. C., Lignell, H., Coggon, M. M., Flagan, R. C., and Seinfeld, J. H.: Vapor wall deposition in Teflon chambers, Atmos. Chem. Phys., 15, 4197–4214,

851   https://doi.org/10.5194/acp-15-4197-2015, 2015.

852 Zhang, Y., Pei, C., Zhang, J., Cheng, C., Lian, X., Chen, M., Huang, B., Fu, Z., Zhou, Z., and Li, M.:

853   Detection of polycyclic aromatic hydrocarbons using a high performance-single particle aerosol mass

854   spectrometer, J. Environ. Sci. (China), 124, 806–822, https://doi.org/10.1016/j.jes.2022.02.003, 2023.

855 Zhang, Z., Wang, H., Chen, D., Li, Q., Thai, P., Gong, D., Li, Y., Zhang, C., Gu, Y., Zhou, L., Morawska,

856   L., and Wang, B.: Emission characteristics of volatile organic compounds and their secondary organic

857   aerosol formation potentials from a petroleum refinery in Pearl River Delta, China, Sci. Total Environ.,

858   584–585, 1162–1174, https://doi.org/10.1016/j.scitotenv.2017.01.179, 2017.

859

860   **Table 1**. Summary of experimental conditions in this study.

Exp	RH	Seed	ΔHC (ppb)[b]	ΔHC ($\mu g\ m^{-3}$)[b]	N_2O_5 (ppb)	HC:N_2O_5 Ratio	ΔM$_O$ ($\mu g\ m^{-3}$)[c,d]	SOA Mass yield (%)[f]
1	<3%	AS[a]	9.5 ± 0.3	40.7 ± 1.4	20	1:2	1.9 ± 0.1	4.5 ± 0.3
2	<3%	AS	15.6 ± 0.5	67.1 ± 2.3	36	1:2	5.4 ± 0.3	8.1 ± 0.6
3	<3%	AS	18.0 ± 0.6	77.6 ± 2.7	40	1:2	6.8 ± 0.4	8.6 ± 0.6
4	<3%	AS	28.4 ± 1.0	122.0 ± 4.3	60	1:2	12.4 ± 0.8	10.1 ± 0.7
5	<3%	AS	48.2 ± 1.7	207.2 ± 7.3	100	1:2	26.1 ± 1.7	12.6 ± 0.9
6	<3%	AS	80.1 ± 2.8	344.4 ± 12.1	160	1:2	48.5 ± 3.1	14.1 ± 1.0
7	<3%	AS	99.1 ± 3.5	426.0 ± 14.9	200	1:2	67.0 ± 4.3	15.7 ± 1.1
8	<3%	AS	155.2 ± 5.4	667.5 ± 23.4	310	1:2	107.4 ± 6.9	16.1 ± 1.2
9	<3%	None	18.2 ± 0.6	78.3 ± 2.7	40	1:2	0.6 ± 0.04	0.8 ± 0.06
10	<3%	None	100.4 ± 3.5	431.8 ± 15.1	200	1:2	47.6 ± 3.0	11.0 ± 0.8
11	50%	AS	17.3 ± 0.6	74.5 ± 2.6	40	1:2	/[e]	/[e]
12	70%	AS	15.8 ± 0.5	67.8 ± 2.4	40	1:2	/[e]	/[e]

[a.] Ammonium sulfate. [b.] Uncertainties in hydrocarbon concentrations are calculated from 3.5% uncertainty in hydrocarbon concentration measured by GC-FID. [c.] Density is 1.35 ± 0.05 g m^{-3}, calculated from the comparison of HR-ToF-AMS and SMPS size distribution data. [d.] Uncertainties in aerosol mass loading are estimated based on uncertainty in aerosol volume concentration measured by the SMPS (5.3%) and uncertainty in SOA density (3.5%). [e.] These numbers are not reported because the density of SOA in humid experiments is not available. [f.] Uncertainties in SOA mass yields are propagated from the uncertainty associated with hydrocarbon concentration and aerosol mass loading.

861

862
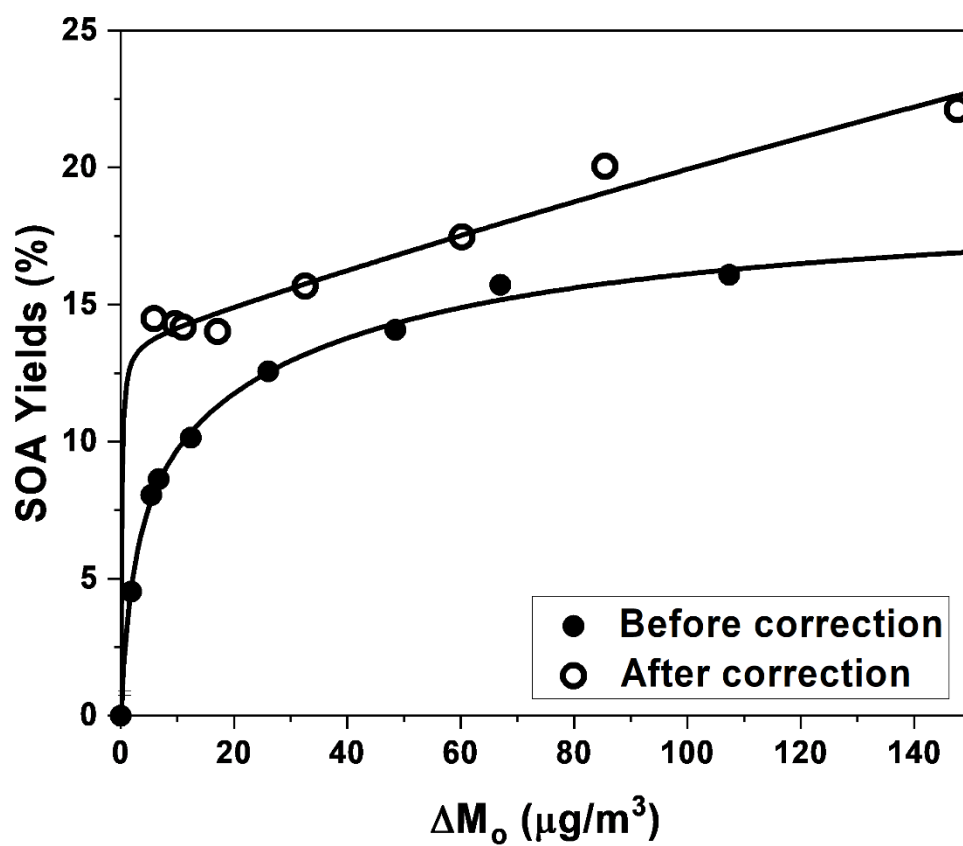
863   **Figure 1.** SOA yield data and yield curves for styrene+NO$_3$ oxidation with and without vapor wall loss

864   correction.
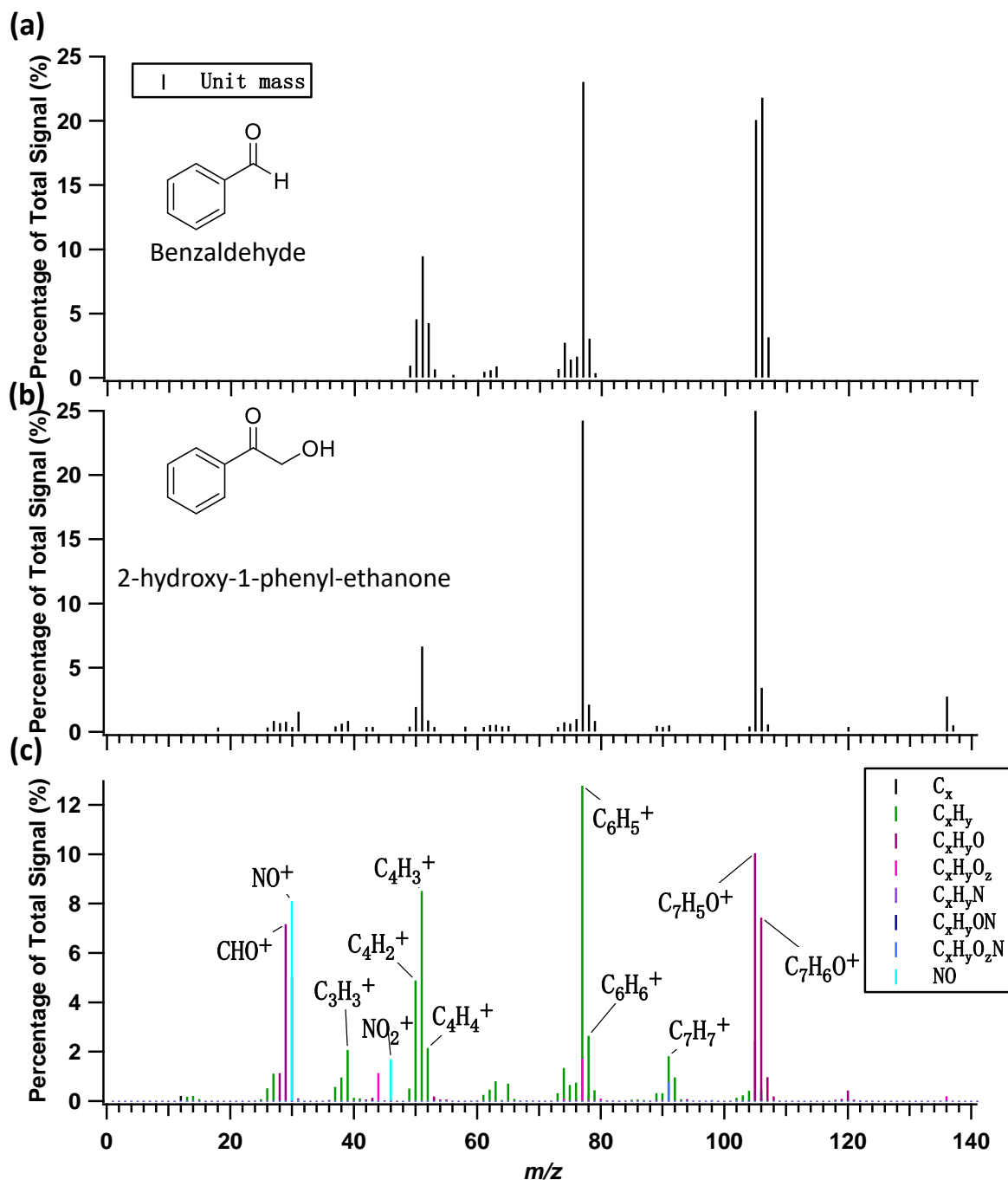
865
Figure 2. Comparison between the National Institute of Standards and Technology (NIST) mass spectra of
866
(a) benzaldehyde; (b) 2-hydroxy-1-phenyl ethenone; and (c) the HR-ToF-AMS mass spectrum (in integer
867
m/z) of SOA from styrene+NO$_3$ oxidation. The chemical structures for benzaldehyde and 2-hydroxy-1-
868
phenyl ethenone are shown in (a) and (b).
869
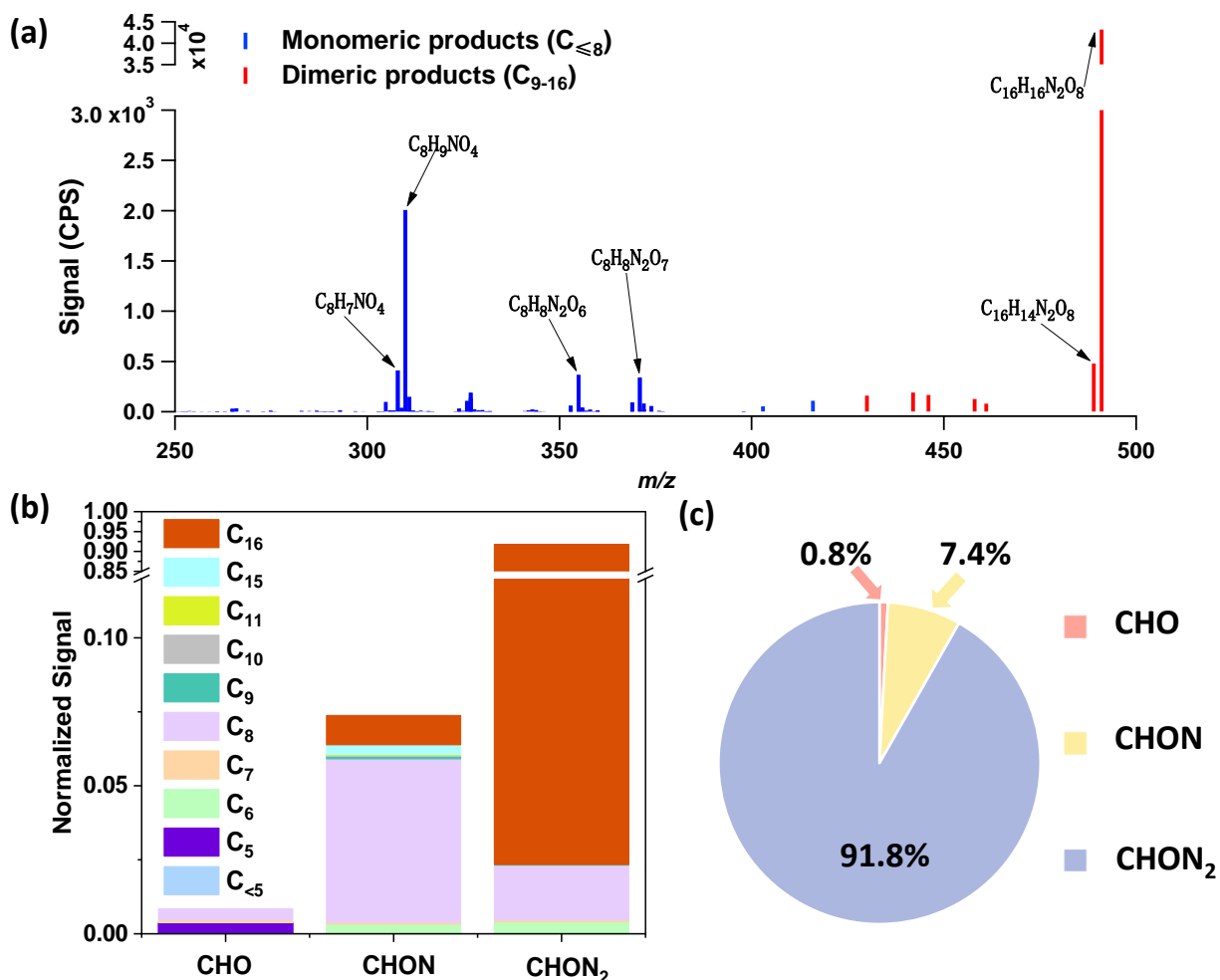
870
871 **Figure 3**. (a) A typical FIGAERO-CIMS mass spectrum of SOA from styrene+NO_3 oxidation (Exp. 7).

872 The sticks are colored to distinguish between monomeric and dimeric products, as indicated in the legend.

873 Prominent masses are labeled with the corresponding chemical formulae without an iodide ion. Only *m/z*

874 250-500 are shown here, there are no specific major products before *m/z* 250 except I^- and HNO_3I^- ; (b)

875 SOA product distribution, categorized by molecule types: CHO, CHON, and $CHON_2$. Each category is

876 further subdivided by carbon number; (c) The pie chart illustrates the relative percentage contributions of

877 CHO, CHON, and $CHON_2$.
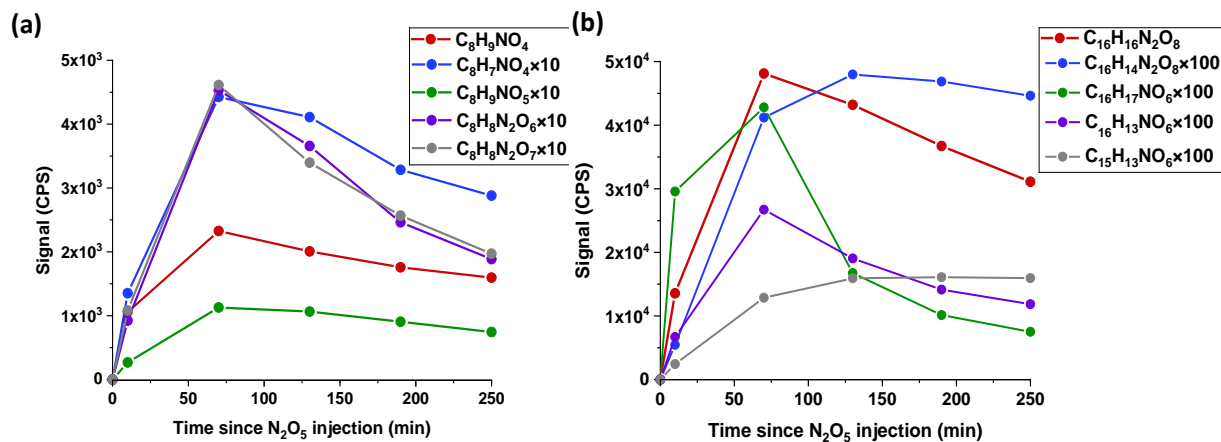
878
879 **Figure 4.** The time series of major particle-phase products from styrene+NO$_3$ oxidation measured by

880 FIGAERO-CIMS (Exp. 7), including: (a) monomeric styrene ONs; and (b) dimeric styrene ONs.

881
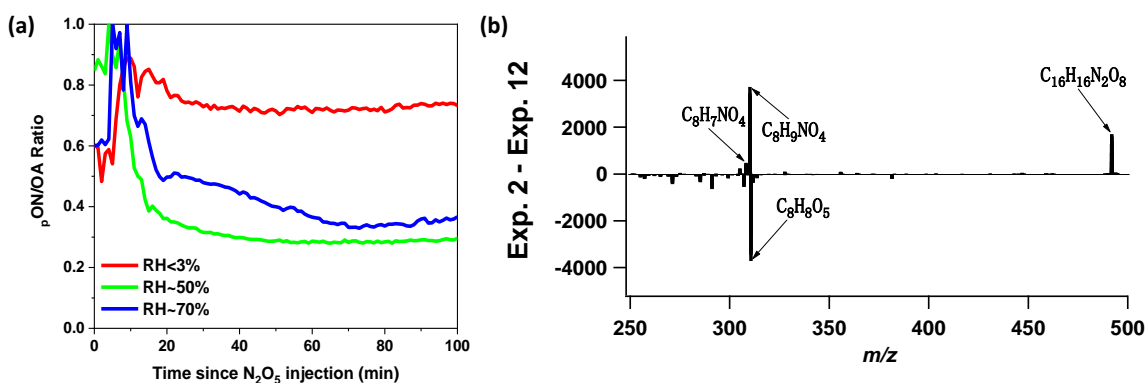
882 **Figure 5. (a)** Time series data of the ratio of particulate ONs ($_p$ON) to total organic aerosols (OA) in

883 Exp. 2 (RH<3%), Exp. 11 (RH~50%), and Exp. 12 (RH~70%); (b) FIGAERO-CIMS difference mass

884 spectrum of SOA: Exp. 2 (RH<3%) minus Exp. 12 (RH~70%). Prominent masses are labeled with the

885 corresponding chemical formulae without an iodide ion.

886

888
889 **Figure 6.** The proposed formation mechanisms for the major particle-phase products resulting from

890 styrene+NO$_3$ oxidation includes two distinct pathways: Pathway A is the proposed formation pathway for

891 monomeric ON products. Pathway B is the proposed formation pathway for dimeric ON products. Radicals

892 A1, A2, and A3 are highlighted in the boxes as the major products resulting from the reaction between

893 aldehydes and NO$_3$ radicals. The nitrooxy peroxy radical is highlighted in yellow as the major RO$_2$ in

894 mechanisms. All chemical structures in the formation mechanisms are proposed based on the molecular

895 formulas of the detected species (shown beneath the structures) or fragments measured by HR-ToF-AMS

896 and require validation through further experiments or theoretical calculations.